NASA CR-168133

EXPERIMENTAL INVESTIGATION OF A HALL-CURRENT ACCELERATOR

Prepared for

LEWIS RESEARCH CENTER

NATIONAL AERONAUTICS AND SPACE ADMINISTRATION

GRANT NSG 3011

by

Gregory M. Plank

January 1983

Approved by

Harold R. Kaufman and Raymond S. Robinson
Department of Physics
Colorado State University
Fort Collins, Colorado 80523

1 Report No	2 Government Accession No	3 Recipient's Catalog No
CR-168133		

4 Title and Subtitle	5 Report Date
EXPERIMENTAL INVESTIGATION OF A HALL-CURRENT THRUSTER (U)	January 1983
	6 Performing Organization Code
7 Author(s)	8 Performing Organization Report No
Gregory M. Plank	
	10 Work Unit No
9 Performing Organization Name and Address	
Department of Mechanical Engineering Colorado State University Fort Collins, Colorado 80523	11 Contract or Grant No NSG 3011
	13 Type of Report and Period Covered
12 Sponsoring Agency Name and Address	Contr. Report
National Aeronautics and Space Administration Washington, DC 20546	14 Sponsoring Agency Code

15 Supplementary Notes

Grant Manager Vincent K. Rawlin
NASA Lewis Research Center
Cleveland, OH 44135

This is a thesis submitted by Gregory M. Plank in partial fulfillment of requirements for the degree of Master of Science, Colorado State University, Spring 1983.

16 Abstract

The Hall-current accelerator is being investigated for use in the 1000-2000 sec. range of specific impulse. Three models of this thruster have been tested. The first two models had three permanent magnets to supply the magnet field and the third model had six magnets to supply the field. The third model thus had approximately twice the magnetic field of the first two. The first and second models differ only in the shape of the magnetic field. All other factors remained the same for the three models except for the anode-cathode distance, which was changed to allow for the three thrusters to have the same magnetic field integral between the anode and the cathode Tests have been conducted on these Hall thrusters to determine the plasma properties, the beam characteristics, and the thruster characteristics. The thruster operated in three modes: (1) main cathode only, (2) main cathode with neutralizer cathode, and (3) neutralizer cathode only. The plasma properties were measured along an axial line, 1 mm inside the cathode radius, at a distance of 0.2 to 6.2 cm from the anode. Results obtained from these tests show that the current used to heat the cathode produced nonuniformities in the magnetic field, hence also in the plasma properties. A Hall thruster of this general design appears to provide the most thrust when operated at a magnetic field less than the maximum value studied.

17 Key Words (Suggested by Author(s))	18 Distribution Statement
Electric propulsion, Electric thruster, Ion source	Unclassified - Unlimited

19 Security Classif (of this report)	20 Security Classif (of this page)	21 No of Pages	22 Price*
Unclassified	Unclassified		

* For sale by the National Technical Information Service, Springfield, Virginia 22161

TABLE OF CONTENTS

INTRODUCTION

Electric propulsion research in the United States has recently been restricted to electrostatic, MPD, and Teflon pulsed plasma thrusters. The electrostatic thruster, with ion acceleration provided by electric fields between closely spaced grids, in particular, appears to meet the needs of interplanetary missions, in which mission times are long.[1-2]

For geocentric missions, a lower range of specific impulse is of more interest, typically 1000-2000 sec. The need for lower specific impulses in geocentric applications results from considerations of mission lifetimes.[3] In interplanetary missions, the added mission time due to the use of electric propulsion is a small fraction of the total mission time. In geocentric missions, however, a mission time of hundreds of days is usually unacceptable when the equivalent chemically propelled mission takes only a few hours.

The most serious obstacle to the use of electrostatic thrusters at low specific impulses (<3000 sec.) is the ion-current limitations of electrostatic acceleration. Work done in the U.S.S.R. has shown that Hall-current acceleration is an alternative to electrostatic acceleration without this limitation.[4]

Hall-current accelerators have been studied as electric thrusters in the past in the U.S., but were dropped because of low efficiency.[5-6] It was, for example, difficult to accelerate more than about one ion downstream for each electron that traveled upstream. This limitation put an upper limit on efficiency of about 50% due to the acceleration process alone. In comparison, the electrostatic thruster has an overall efficiency of about 70% at 3000 sec., and is capable of higher efficiencies at higher specific impulses. This relatively poor performance of the Hall-current accelerator, at high specific impulses that were then being considered, resulted in its demise in the U.S. in about 1970.

If we consider low specific impulses, though, the relative performance of the Hall-current accelerator is at much less of a disadvantage. As indicated above, the electrostatic thruster becomes increasingly limited in ion-current capacity as specific impulse is reduced. The Hall-current accelerator has no such limitation. The electron backflow results in a serious loss at high specific impulses. But at low specific impulses this backflow is more easily recovered by using it to generate ions.

The investigation of the Hall-current accelerator reported herein was undertaken as a part of a preliminary attempt to re-evaluate this type of thruster for electric propulsion. The preliminary nature of this investigation should be emphasized. It has been over a decade since the Hall-current accelerator was last seriously considered for electric propulsion in the U.S.

DESIGN CONSIDERATIONS

The design of the Hall-current accelerator is based on the Lorentz force equation for a charged particle moving in magnetic and electric fields.

$$\vec{F} = q(\vec{E} + \vec{v}x\vec{B}) \tag{1}$$

This equation indicates that if an electron acquires a velocity in the direction perpendicular to a magnetic field then a force will be applied to the electron at a right angle to the perpendicular component of the velocity and the direction of the magnetic field. Thus, if an electron has a velocity directed along the axis in a cylindrical radial magnetic field, the electron will acquire a circumferential velocity about the axis.

The simplest geometry for a Hall-current accelerator is an acceleration channel in the shape of an annular ring with one of the pole pieces in the center and the other the outer wall. This arrangement is indicated in Figs. 1(a) and 1(b). If the anode is placed at one end, the upstream end, then an electrical field will be established with the electric field vector directed downstream from the anode. Positive ions will be accelerated in the direction of the electric-field vector, while electrons will experience a force in the opposite direction. The force on the electrons will, of course, result in their precession about the axis. Diffusion toward the anode will take place as the result of collisions during this precession. Most of these collisions are believed to be due to "turbulence" in the plasma.[7] As the anode is approached, the electron energy will tend to increase, resulting in an increased probability that an ionizing collision will take place. With collisions taking place the increase in electron energy will translate into an increase in electron temperature.

From the viewpoint of obtaining a high acceleration efficiency (a high ratio of accelerated ion current to electron current flowing in the opposite direction), a high magnetic field strength is desired in the acceleration channel. At the same time, efficient use of the electron energy to produce ions, as the electrons approach the anode, requires a low magnetic field strength near the anode. This variation of field strength is obtained by having the pole pieces farther apart near the anode, and closer together at the downstream end of the acceleration channel, as indicated in Fig. 2(a). With an upstream "discharge chamber" cathode this design also offers a low magnetic field integral

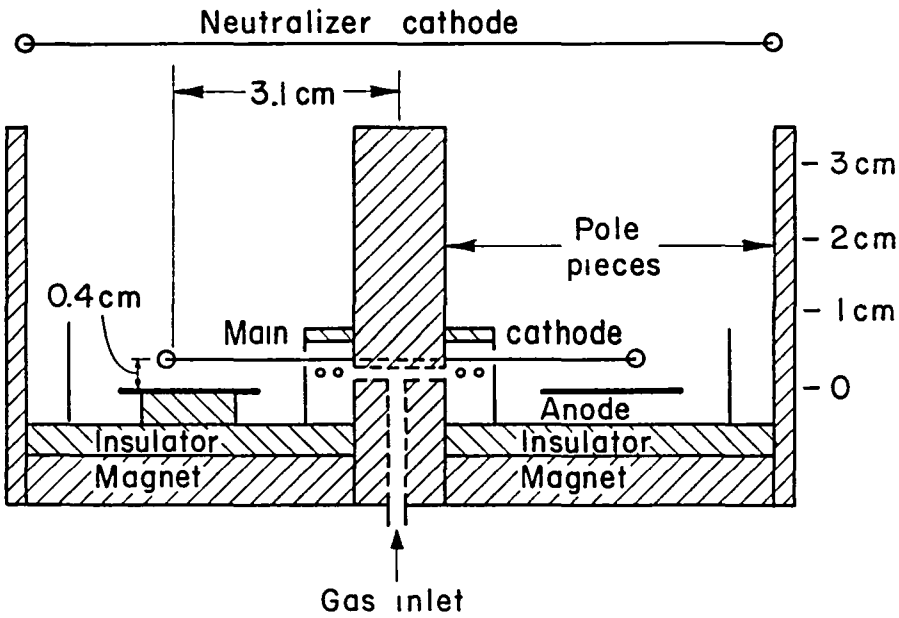

(a) Side view.

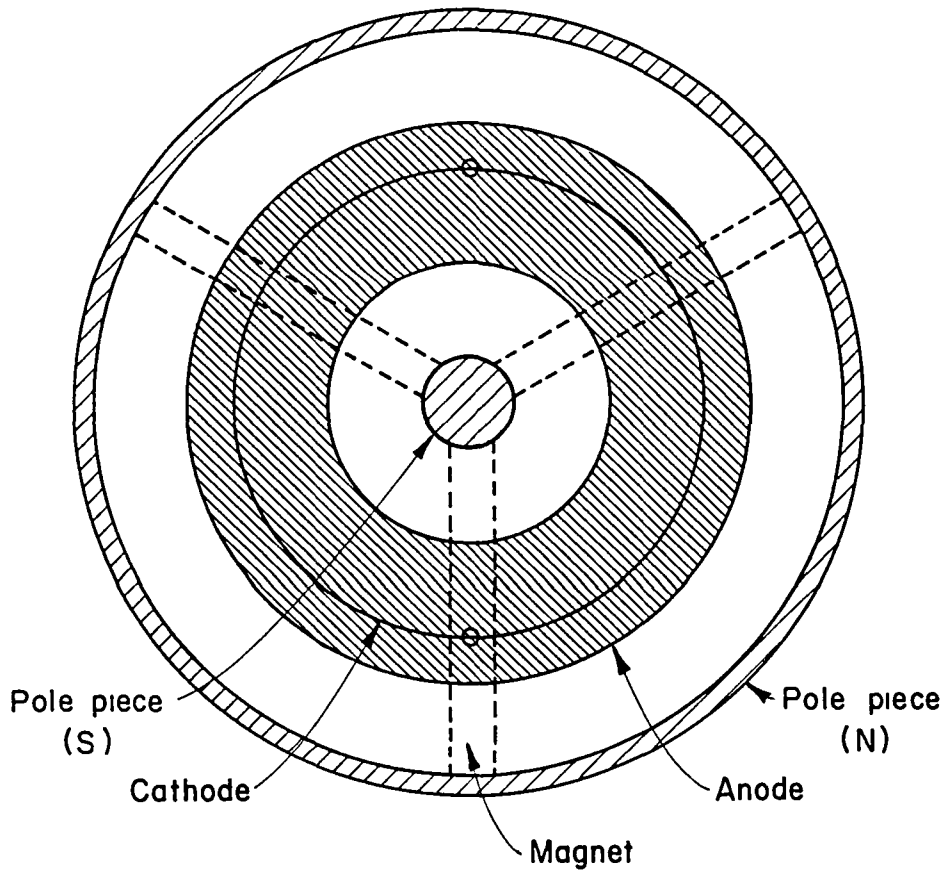

(b) End view.

Fig. 1. Drawings of the Hall-current thruster, three magnets with parallel pole pieces.

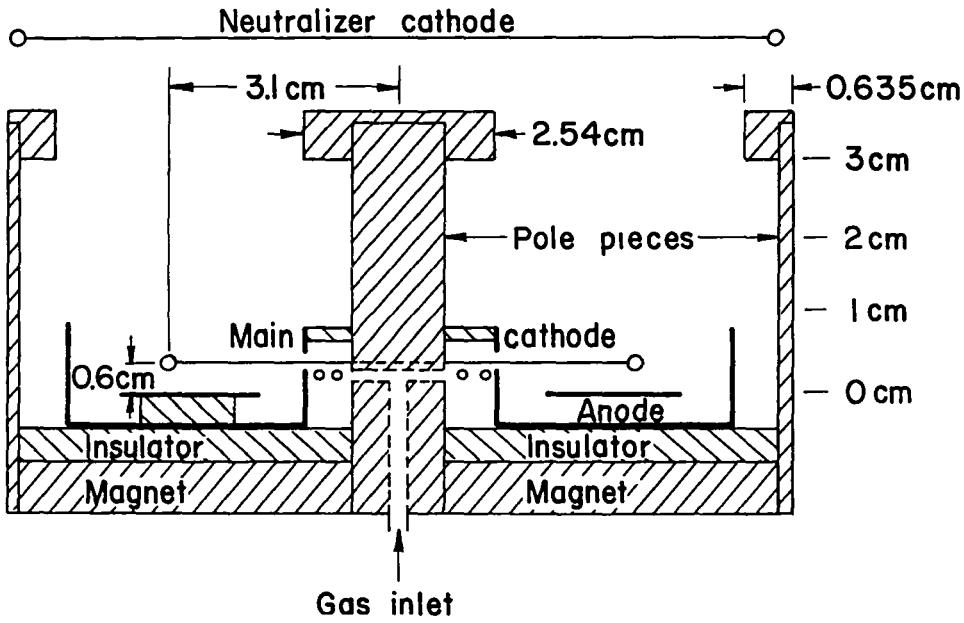

(a) Side view.

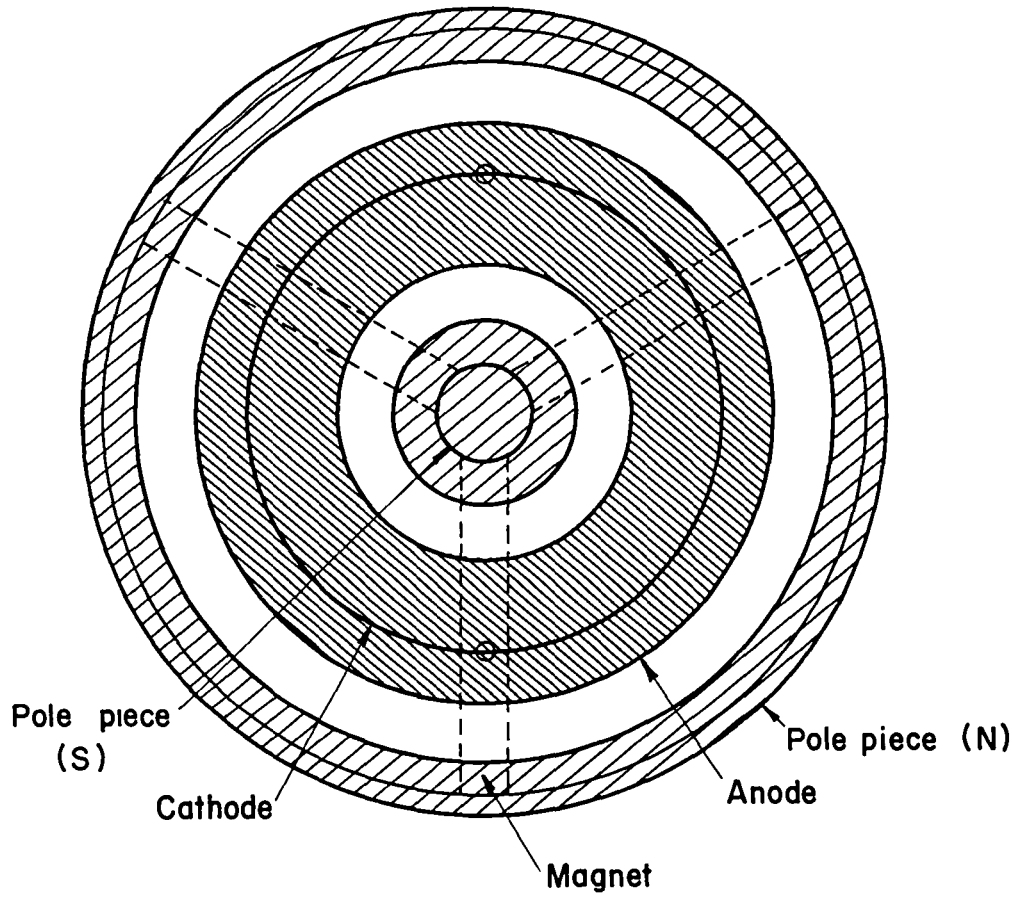

(b) End view.

Fig. 2. Drawings of Hall-current thruster, three and six magnets with modified pole pieces.

between the anode and this cathode for ease in starting. The shape of the magnetic field in a Hall-current thruster is thus equivalent in importance in an electrostatic thruster to the magnetic design of the discharge chamber plus the design of the grids.

APPARATUS

Construction

The Hall-current thruster investigated herein, indicated in Figs. 1 and 2, uses two cylindrical magnetic poles to generate an essentially radial magnetic field. As indicated in Figs. 1 and 2, a nonmagnetic annular anode was located at the upstream end of the acceleration channel. A nonmagnetic annular cup, to contain the discharge, surrounded the anode. Two refractory metal cathodes were used, one located near the anode (main or discharge cathode), and the other approximately one centimeter beyond the exit plane of the acceleration channel (neutralizer cathode), as indicated in Figs. 1(a) and 2(a). The main cathode was fabricated of 0.51 mm diameter W, with an emission of 1 A for a nominal 17.5 A heater current. (The two semicircular segments of this cathode were effectively in parallel, resulting in a heater power supply current of 35 A.) The neutralizer cathode was two strands of 0.25 mm diameter W wire with an emission of 1 A for a nominal 6 A heater current. The propellant (Ar) was introduced through the central pole piece, and a propellant distributor geometry was used to achieve a circumferentially uniform gas flow into the ion-production region. To further assure uniformity, rings of insulator (mica) were used to force the propellant through 19 evenly distributed small holes in the inner cylinder of the annular cup, Figs. 1(a) and 2(a). The second and third models of the thruster were modified by the addition of a soft iron cap 2.54 cm in diameter by 0.64 cm thick over the center pole piece, and a soft iron ring 8.89 cm inside diameter by 10.16 cm outside diameter by 0.64 cm thick inside the outer pole piece, thereby producing a constriction in the downstream end of the magnetic field.

For the work described herein, three models of the thruster were tested, the first with the thruster as described using three evenly spaced magnets with parallel pole pieces, Fig. 1(a). The second was the same basic thruster but with its pole pieces modified as indicated in Fig. 2(a). The third was the same thruster as the second, except that instead of three magnets it had six evenly spaced magnets. The magnets were made of Alnico V and were 0.6 cm in diameter by 4.6 cm in length. (These magnets were remagnetized in a 1 T field before use.)

Magnetic Field

The magnetic integral in a radial-field configuration varies with the radius at which the integration is performed. Still, the concept of the magnetic integral is a useful one for general design considerations. For the work described herein the magnetic integral between the anode and main cathode, at the main cathode radius, was set to be 20×10^{-6} T-m (20 Gauss-cm) for all tests on the three models. (This integral value requires that the anode-cathode spacing be approximately 4 mm for the three magnet thruster with parallel pole pieces, 6 mm for the three magnet thruster with modified pole pieces, and 3 mm for the six magnet thruster with modified pole pieces.) This value is low compared to the typical $50\text{-}60 \times 10^{-6}$ T-m between the anode and cathode in an electron-bombardment discharge chamber. The low integral value used was selected after a magnetic integral of 60×10^{-6} T-m was tried, but proved impossible to operate in the <100 V range that was felt to be of interest.

The magnetic field of the operating Hall-current thruster had two major components to the local field strength. First there was the essentially radial magnetic field produced by the magnets and the cylindrical pole pieces. The strength of this component is indicated in Figs. 3, 5, and 7 for the thrusters wtih three-magnet parallel pole pieces, three-magnet modified pole pieces, and the six-magnet modified pole pieces. These figures show contours of constant magnetic field strength at the axial locations midway between the anode and main cathode. Figures 9(a), 10(a), and 11(a) show the mean axial variation of the magnetic field strength of the thrusters.

The second major component was the contribution due to the main cathode's heater current. (To avoid the problem of measuring the magnetic field close to a current carrying element, the main cathode field component was calculated.) Figures 4, 6, and 8 show the effect that a 17.5 A heater current would have on the field strengths shown in Figs. 3, 5, and 7, respectively. Figures 9(b), 10(b), and 11(b) show the effect that a 17.5 A heater current would have on the axial field strength 1 mm inside the cathode radius of the thrusters with three-magnet parallel pole pieces, three-magnet modified pole pieces, and six-magnet modified pole pieces.

The main cathode heater current clearly has a significant effect on the magnetic field distribution. On one side of the thruster the 17.5 A heater current reduces the anode-cathode magnetic integral from 20×10^{-6} T-m to approximately 10×10^{-6} T-m and on the other side increases it to approximately 30×10^{-6} T-m. (The magnetic field integral with no cathode heater current was 20×10^{-6} T-m.)

This significance of the heater current appears to be a sharp distinction from electro-bombardment thruster experience. In the latter, the background field near a refractory cathode is normally quite small. Inasmuch as the cathode heater current is not enough to result in localized containment of the emitted electrons, the effect of the heater current on discharge-chamber performance is usually insignificant.

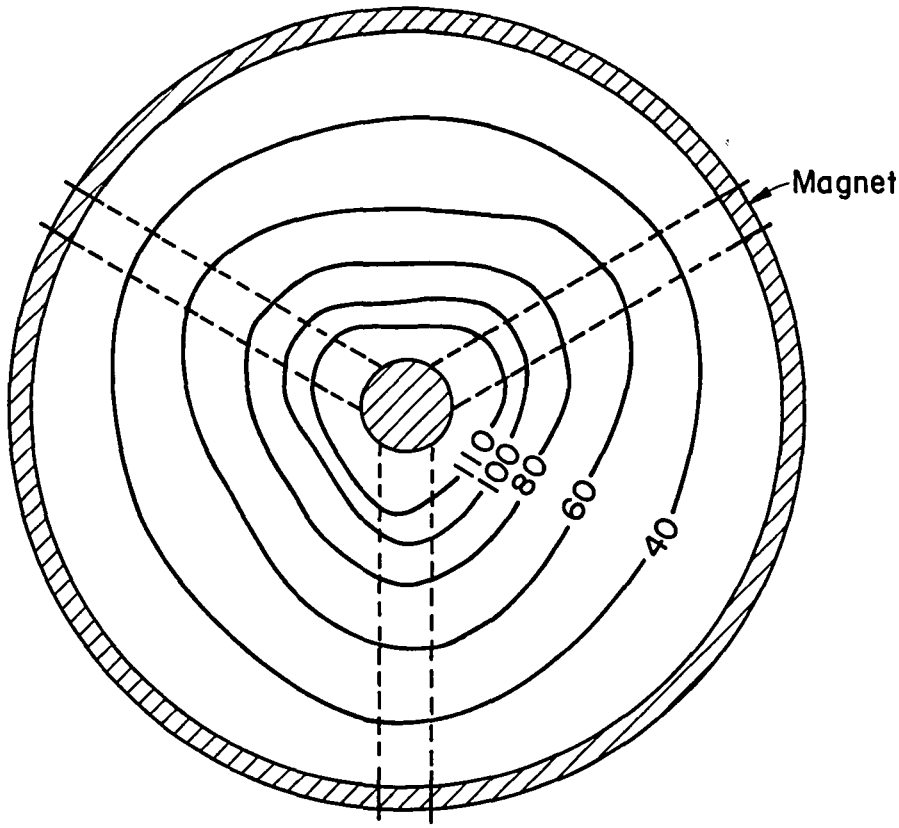

Fig. 3. Contours of constant magnetic field strength, axial location 2 mm. (Field strength indicated in Gauss. Cathode not operating.) Three magnets with parallel poles.

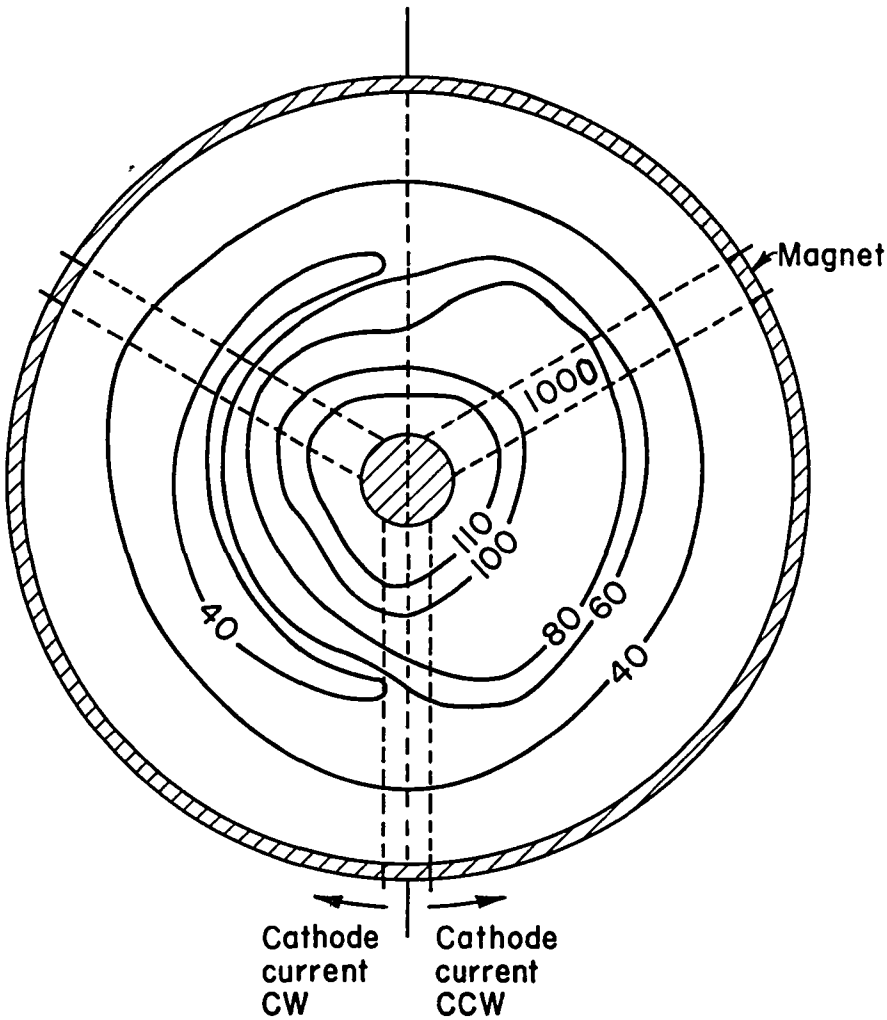

Fig. 4. Contours of constant magnetic field strength, axial location cathode plus 1 mm. (Constant field of Fig. 3 plus the calculated effect of 17.5 A current through each branch of the cathode, field strength indicated in Gauss.)

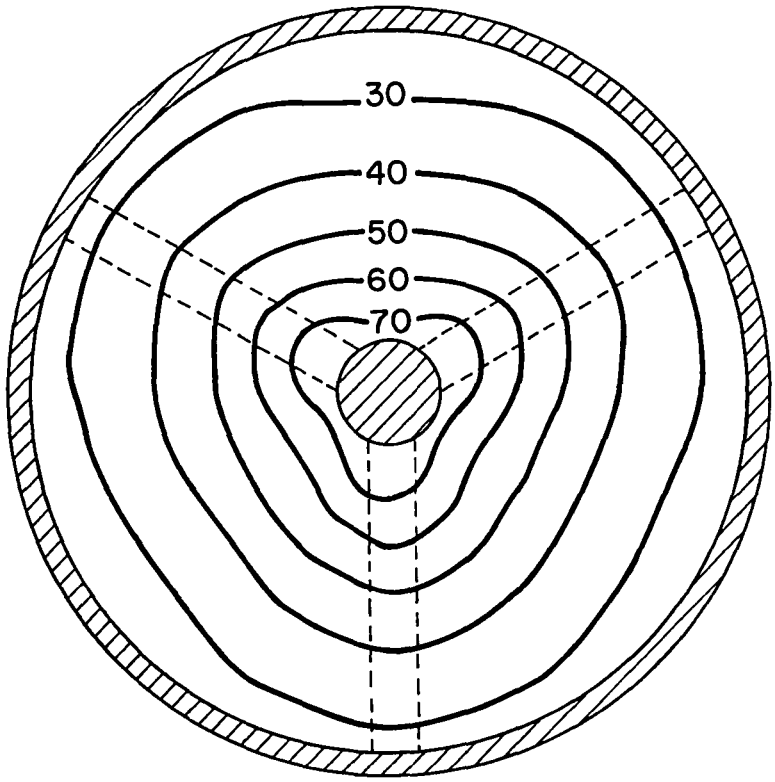

Fig. 5. Contours of constant magnetic field strength, axial location 2 mm. (Field strength indicated in Gauss. Cathode not operating.) Three magnets with modified poles.

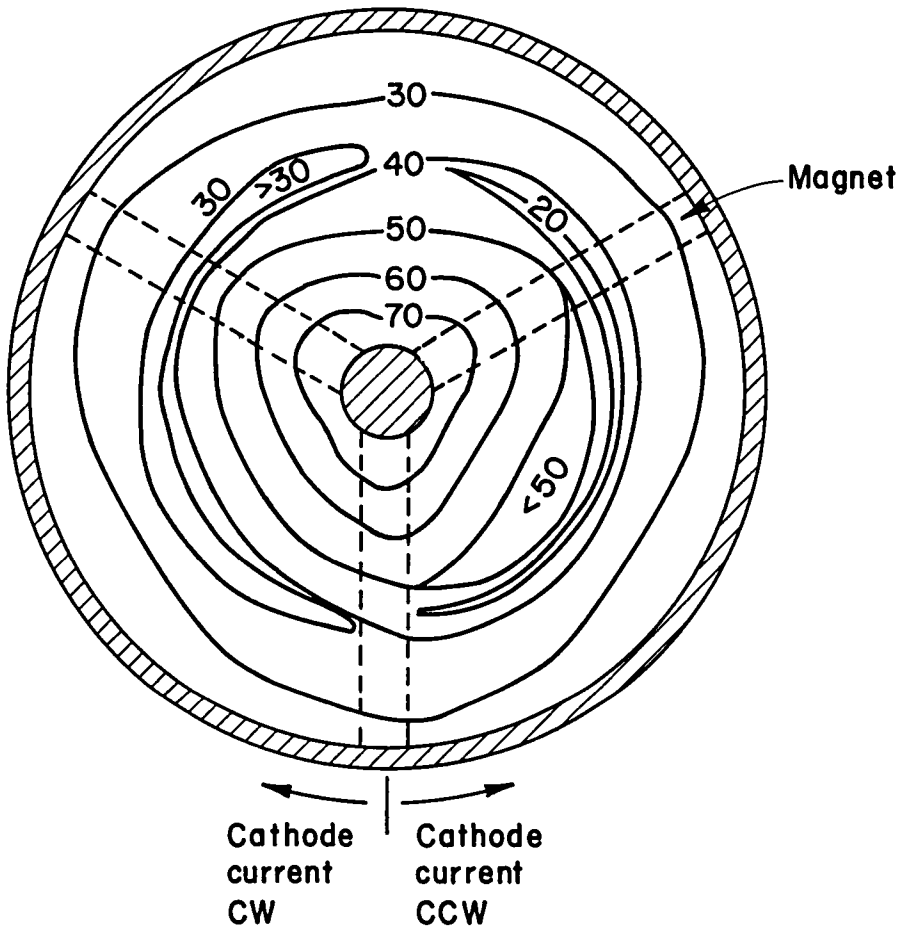

Fig. 6. Contours of constant magnetic field strength, axial location cathode plus 1 mm. (Constant field of Fig. 5 plus the calculated effect of 17.5 A current through each branch of the cathode, field strength indicated in Gauss.)

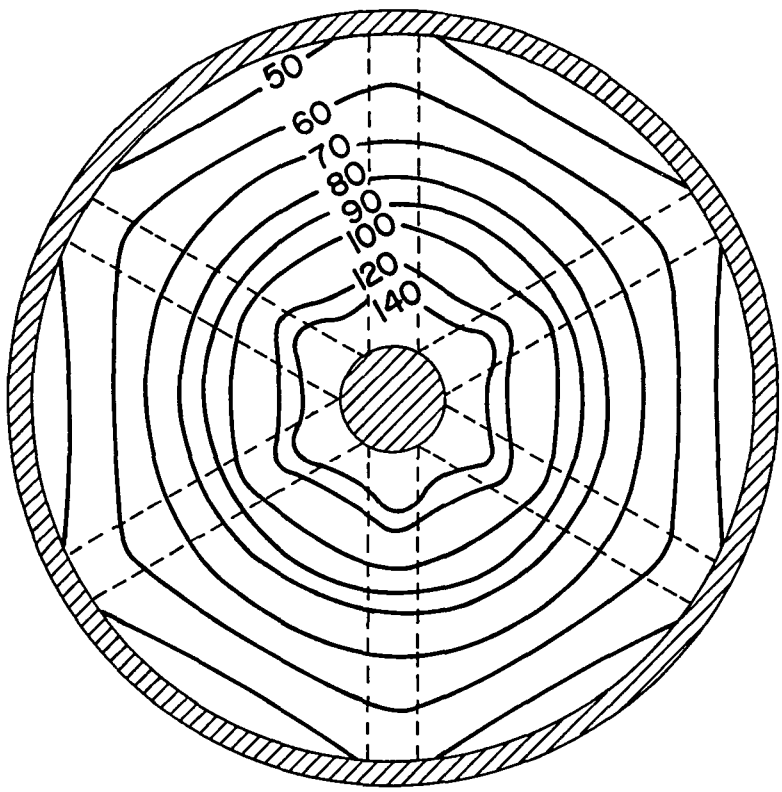

Fig. 7. Contours of constant magnetic field strength, axial location 2 mm. (Field strength indicated in Gauss. Cathode not operating.) Six magnets with modified poles.

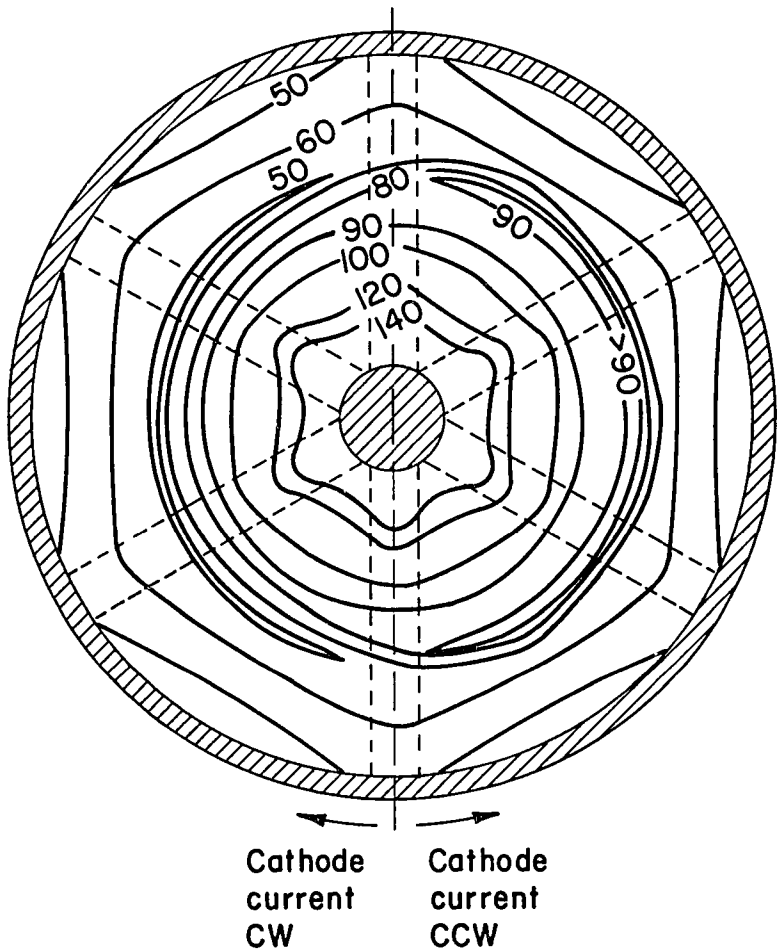

Fig. 8. Contours of constant magnetic field strength, axial location cathode plus 1 mm. (Constant field of Fig. 7 plus the calculated effect of 17.5 A current through each branch of the main cathode, field indicated in Gauss.)

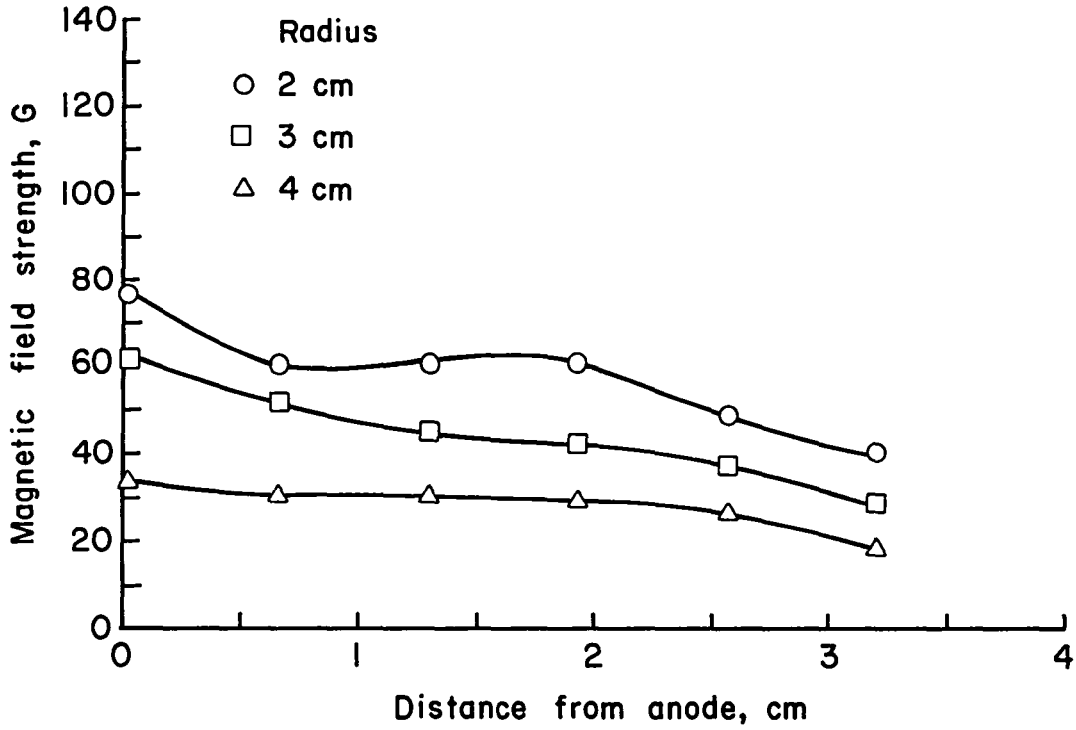

(a) Cathode not operating.

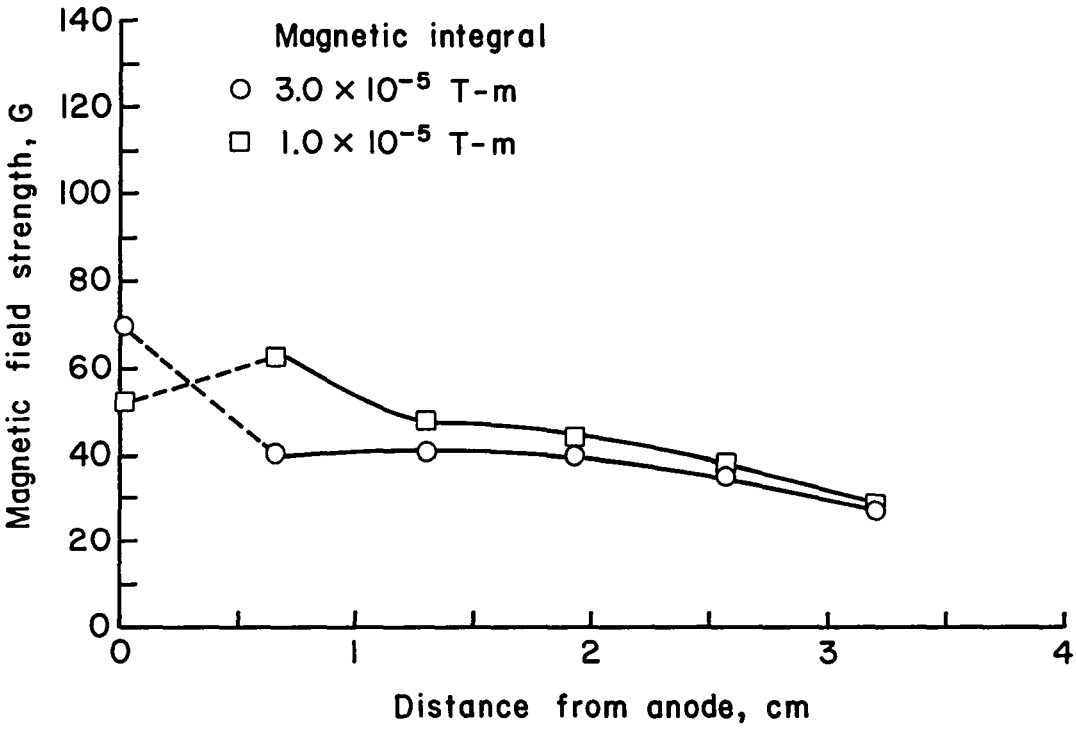

(b) Constant field plus the effect of ±17.5 A cathode current.

Fig. 9. Mean axial variation of magnetic field strength at 1 mm inside the cathode radius. (Three magnet thruster with parallel pole pieces.)

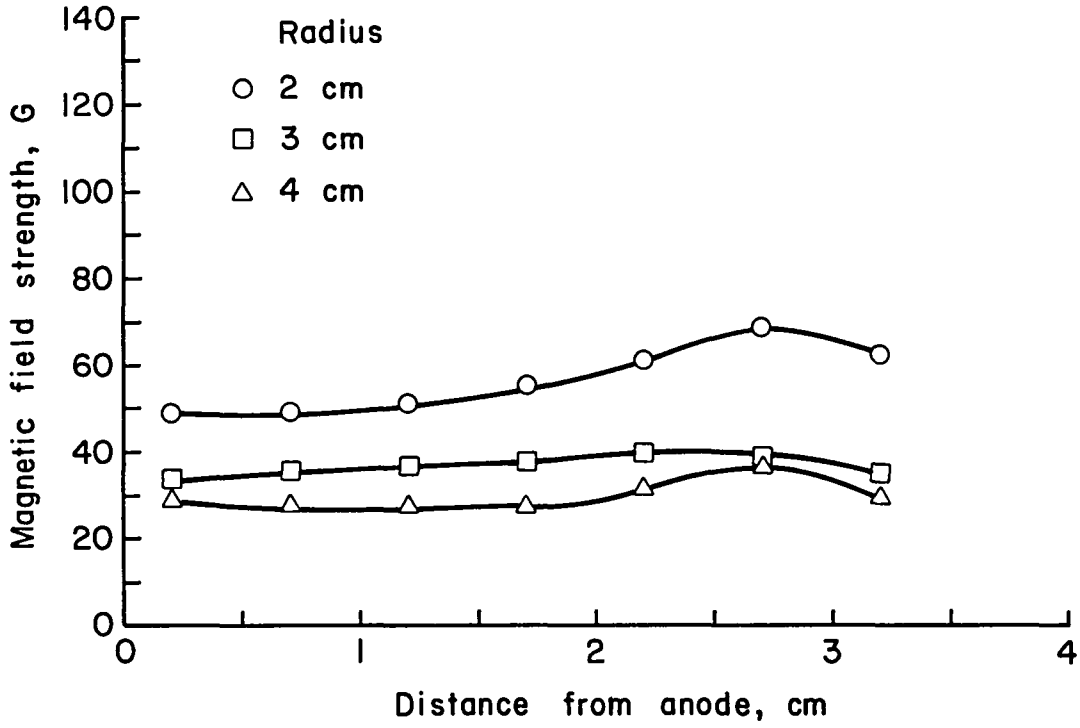

(a) Cathode not operating.

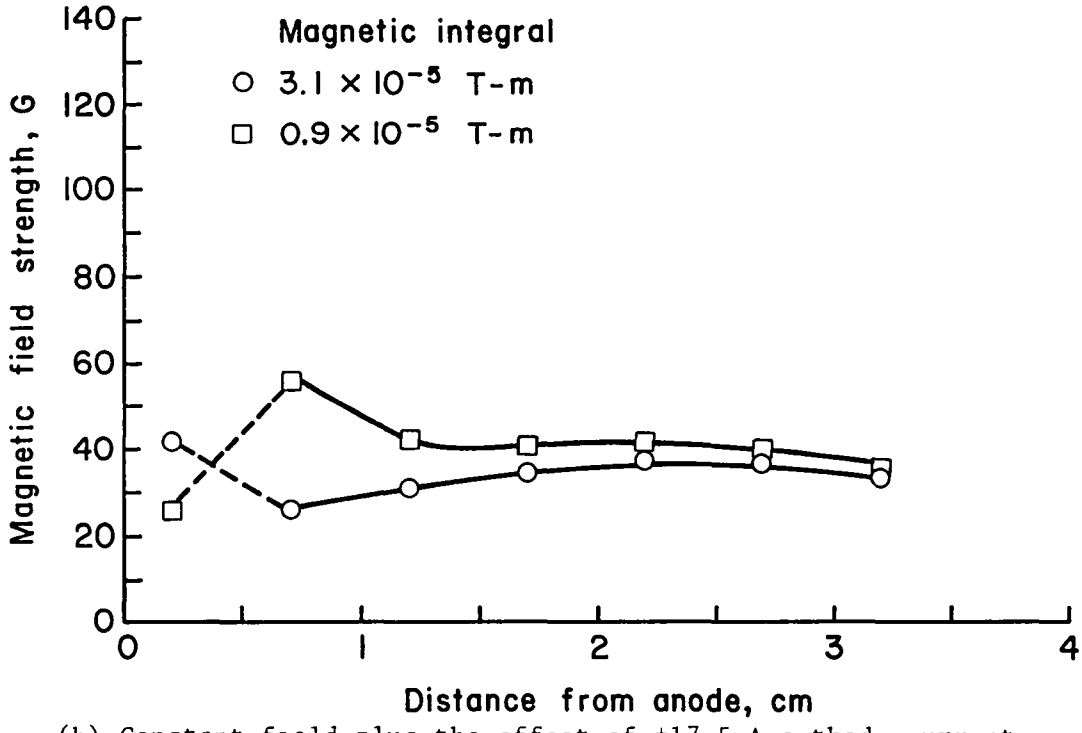

(b) Constant field plus the effect of ±17.5 A cathode current.

Fig. 10. Mean axial variation on magnetic field strength at 1 mm inside the cathode radius. (Three magnet thruster with modified pole pieces.)

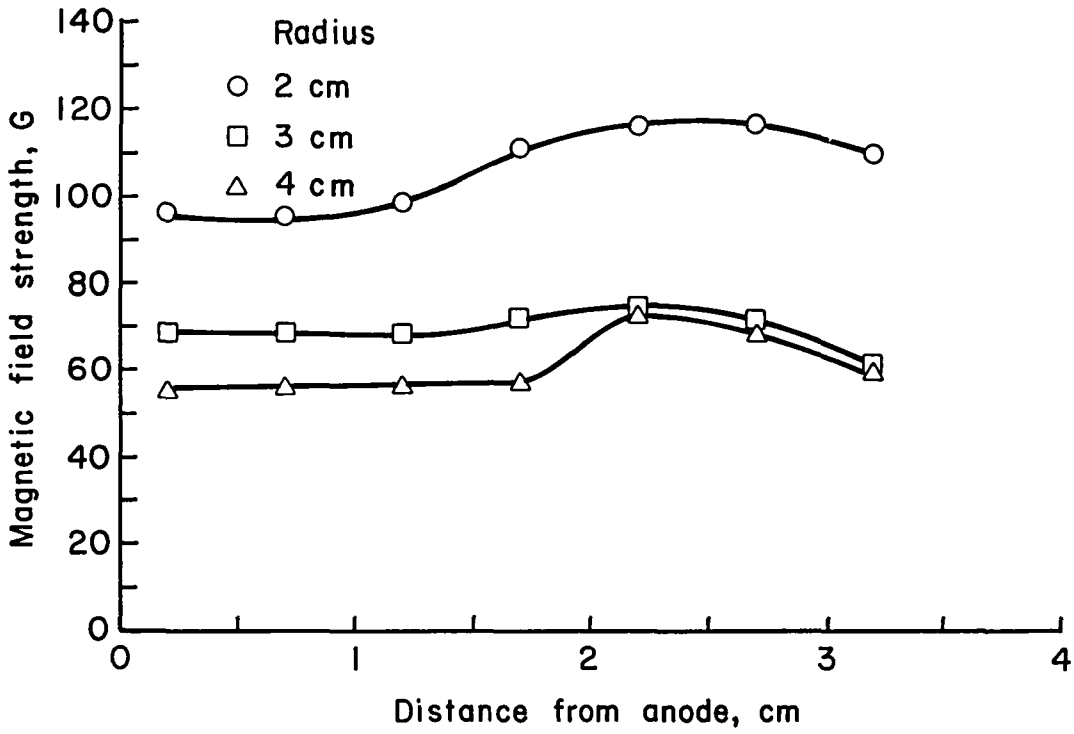

(a) Cathode not operating.

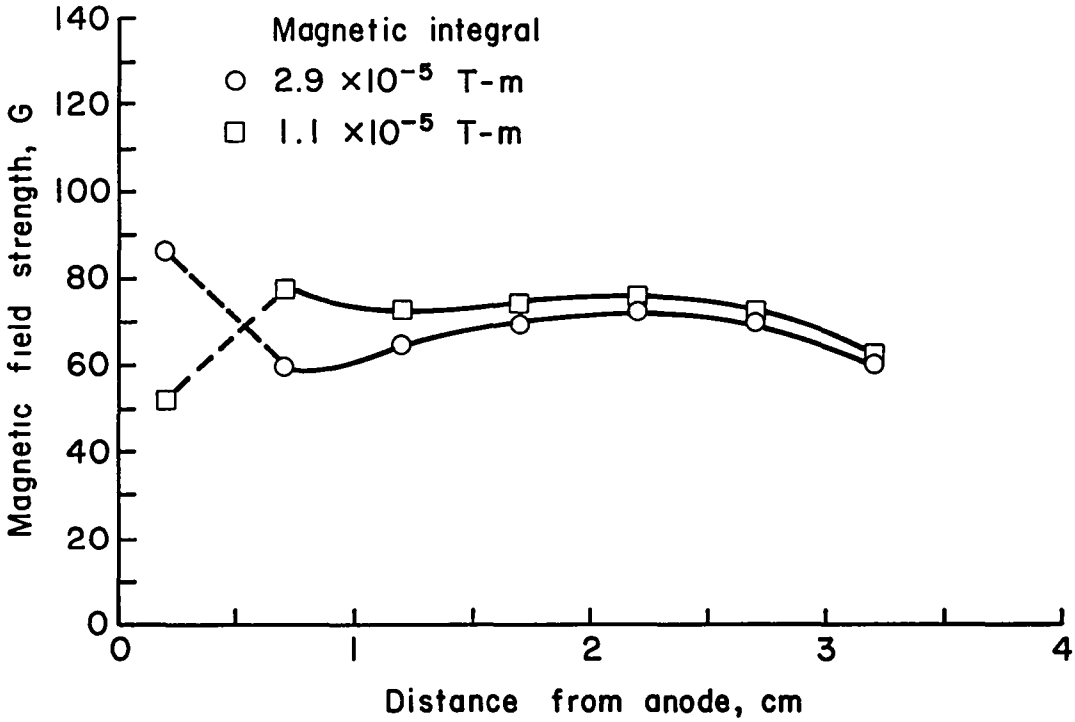

(b) Constant field plus the effect of ±17.5 A cathode current.

Fig. 11. Mean axial variation of magnetic field strength at 1 mm inside the cathode radius. (Six magnet thruster with modified pole pieces.)

Operation

The Hall-current thruster design tested can be operated in three different modes: main cathode only, main cathode and neutralizer cathode together, and neutralizer cathode only. The electrical circuitry for all three modes is indicated in Fig. 12. For flows of propellant of about 100-1000 mA-equiv., the vacuum chamber pressure was in the range of $1\text{-}10 \times 10^{-4}$ Torr. (The relation between flow rate and pressure was close to linear.)

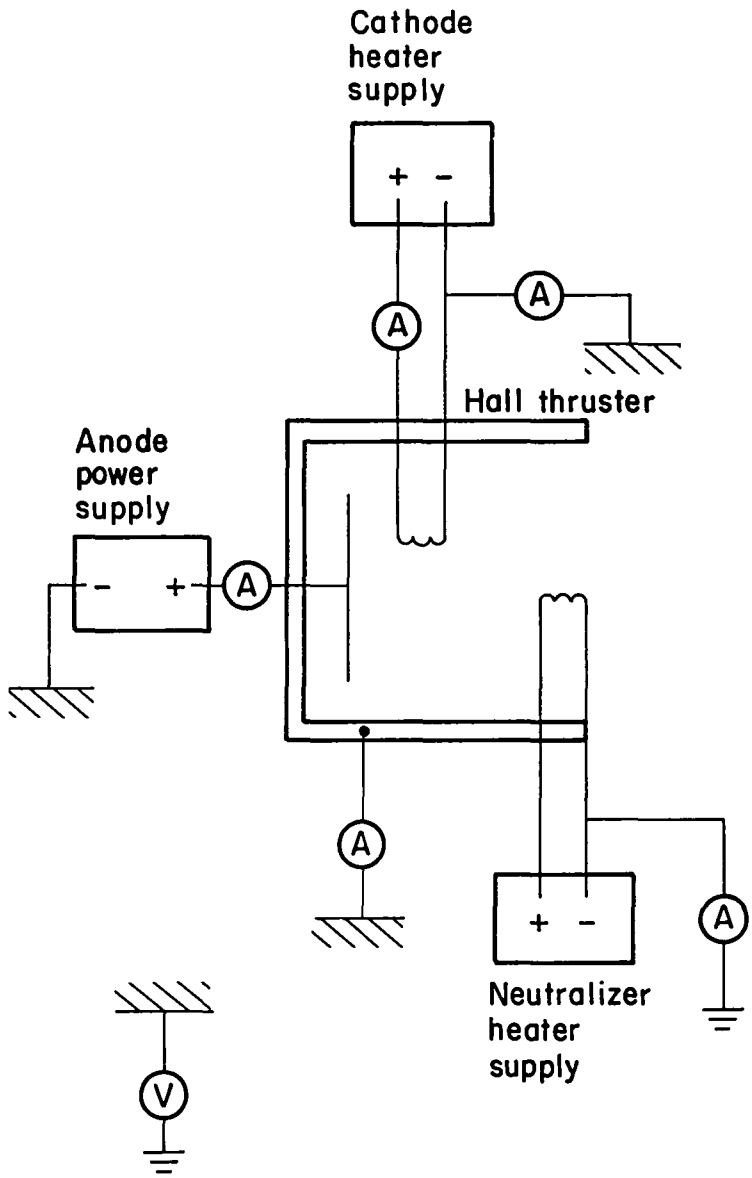

Fig. 12. Electrical power schematic.

PROCEDURE

The following procedure was used to test the Hall-current accelerator. The operating range was determined by exploring the range of anode voltages for which the discharge could be maintained for the three operating modes, over a range of pressures from 3×10^{-4} to 9×10^{-4} Torr. To determine the plasma profile, Langmuir probe traces were taken at selected positions and operating conditions. (The Langmuir probe was cleaned by ion and electron bombardment before each trace was taken.) To determine the overall performance of the thruster, Faraday cup measurements were taken to determine the ion beam current at selected axial and radial positions; this determined both the beam spread and the beam attenuation. Also, Faraday cup measurements were taken to measure the beam energy profile.

INSTRUMENTATION

The instruments used were a Langmuir probe and a shielded Faraday cup. Both the Langmuir probe and the Faraday cup had a variable bias placed on the collecting element. The output from each device was registered on an X-Y recorder. The Langmuir probe was used to determine the plasma properties and the Faraday cup was used to determine the beam current and the beam energy.

Langmuir Probe

The Langmuir probe works by collecting the ions and electrons which intercept the probe sheath. The energies of particles were selected by placing a bias on the probe element with respect to the plasma potential. The bias acts as a selection device by rejecting the particles which were not energetic enough to overcome the potential gradient of the sheath. The probe used was a Ta wire 0.254 cm long by 0.0762 cm in diameter; these values were ±0.00127 cm.

Analysis of the probe data was accomplished using the thin sheath analysis approximation. This approximation can be used if the thin sheath criterion is met, $s - a << a$ where:

$$s - a = \frac{4\varepsilon_o}{9} \left(\frac{2q}{m}\right)^{1/2} \frac{V^{3/2}}{j} \left(1 + \frac{2.66}{\sqrt{\eta}}\right)^{1/2} \qquad (2)$$

and

$$\eta = eV/kT$$

where "a" is the diameter of the probe.[8] In the region of interest $s - a = 6 \times 10^{-10}$ m and since $a = 7.4 \times 10^{-4}$ m the thin sheath criterion was satisfied. Thus the thin sheath approximation could be used.

There are potential problems introduced in the Langmuir probe analysis when the measurements are taken in a magnetic field. These are encountered as a result of the Larmor radius of the electrons being approximately equal to or less than the probe diameter and as a result of the Hall current velocity being of the same order as the random

electron velocity. The Larmor radius was found to be approximately 1.3 cm in the strongest magnetic field region, therefore a $<< \lambda_L$. Thus this effect of the magnet field did not have a significant effect on the probe current.

The Hall current velocity can be estimated to the first order by equating the Hall current and the magnetic field to the thrust.

$$\vec{T} = \vec{I} \times \vec{B} \tag{3}$$

Langmuir probe measurements indicated that most of the Hall current was in the high magnetic field region of the exit plane and near the outer radius. Therefore, as an estimate on the Hall current, in the axial line in which the presented data was taken, the total current was divided into two regions. The region of interest comprised approximately 91% of the area, perpendicular to the Hall current, and 15% of the total Hall current. Using these values the Hall current velocity was calculated to be approximately 5×10^3 m/sec. The random thermal velocity was approximately 2×10^6 m/sec, therefore, the Hall current velocity did not significantly affect the collected current.

The major uncertainties were the measured probe area (±2.25%), the X-Y recorder (±3%) and an unknown amount of error due to the effect of the probe shield depressing the local plasma density, a change in the probe area due to deposition or sputtering, surface layers which would change the work function of the probe, and errors due to interpreting the data. However, overall there should not be more than about 12% error in the Langmuir probe data.

Faraday Cup

A shielded Faraday cup was used to measure the beam characteristics. The construction of this probe had to take into account the electron density and temperature, of the beam and the amount of current to be collected. To adequately shield the current collecting element from electrons, the size of the holes in the electron shielding screen must be less than or equal to $2\lambda_D$. At the position of the Faraday cup λ_D was approximately 100 μm, therefore, a screen having holes approximately 200 μm in diameter will give adequate shielding. The shield used was a 125 Hex micromesh screen having a hole size of 172.5 μm and an open area fraction of 70%. Thus the screen provided a sufficient amount of shielding to prevent thermal electrons from being collected.

The maximum current density to be measured by the collector can be determined by considering Child's law limit. If a current density of 62.5 A/m^2 was to be measured using a minimum voltage difference of 60 V then a screen-to-probe distance of not more than 2.54×10^{-4} m could be used. The Faraday cup constructed had a shield-to-collector distance of 2.54×10^{-4} m and was used with a negative 60 V bias on

the shield, therefore a current density of 62.5 A/m^2 could be accurately measured. The maximum current measured by this Faraday cup was approximately 50 A/m^2, thus the Faraday cup was suitable for accurately measuring the beam currents.

The measurements obtained by the Faraday cup had errors introduced by uncertainties in the size of the current collecting element, the open area fraction of the screen, the amount of secondary electron emission from the electron shield, and the accuracy of the metering. The current collecting element was 0.635 cm ± 0.00127 cm in diameter; this could introduce an error of approximately 1/2% in the probe area. The error from secondary electron emission considerations was introduced by Ar ions striking the Ni screen and producing an emission of electrons. A portion of these electrons will reach the current collecting element causing the measured current to be lower than it should be. For Ar^+ ions striking Ni approximately 3.5% of the ions hitting the Ni will produce a secondary electron at the energies of interest.[9] The maximum current of secondary electrons, therefore, depends on the ion current density and the area of screen that intercepts the beam. For this Faraday cup an error of up to 1.5% could be produced by secondary electrons. The error in the X-Y recorder was approximately 3%. Therefore, the total error for the Faraday cup current measurements was approximately +4.9% and -3.4%. The error in the energy measurements was ±3% since the energy measurements did not depend on the magnitude of the current.

EXPERIMENTAL RESULTS

Operating Range

The operating ranges for the thruster with three-magnets and parallel pole pieces, Figs. 13 and 14, indicate at what discharge voltage the discharge initiated and extinguished over a range of system pressures.

The main cathode only mode was seen to initiate a discharge with a current of 2.5 A at a discharge voltage of

$$V = 80 - 3.9 \times 10^4 P \quad (4)$$

and extinguish at a voltage of

$$V = 47 - 1.8 \times 10^4 P \quad (5)$$

where P is the system pressure in Torr, over the range of $3.5 - 8 \times 10^{-4}$ Torr. When the neutralizer cathode was also used, at a temperature sufficient to emit 1 A, the discharge was initiated at approximately the same voltage as in Eq. (4). The voltage at which the discharge was extinguished, however, had two distinctly different characteristics at high and low system pressures. At low pressures $3.5 - 6.5 \times 10^{-4}$ Torr, the discharge was extinguished at a voltage of

$$V = 81 - 4.5 \times 10^4 P \quad (6)$$

while at high pressures $7 - 8 \times 10^{-4}$ Torr, it extinguished at a voltage of

$$V = 53 - 1 \times 10^4 P \quad . \quad (7)$$

(The data from which Eqs. (4) through (7) were obtained are shown in Fig. 13.) While operating in the neutralizer cathode only mode (where the discharge was initiated using the main cathode, which was then turned off) with a neutralizer emission of 1.5 A the discharge with a current of 2.0 A could be maintained as indicated by the shaded region

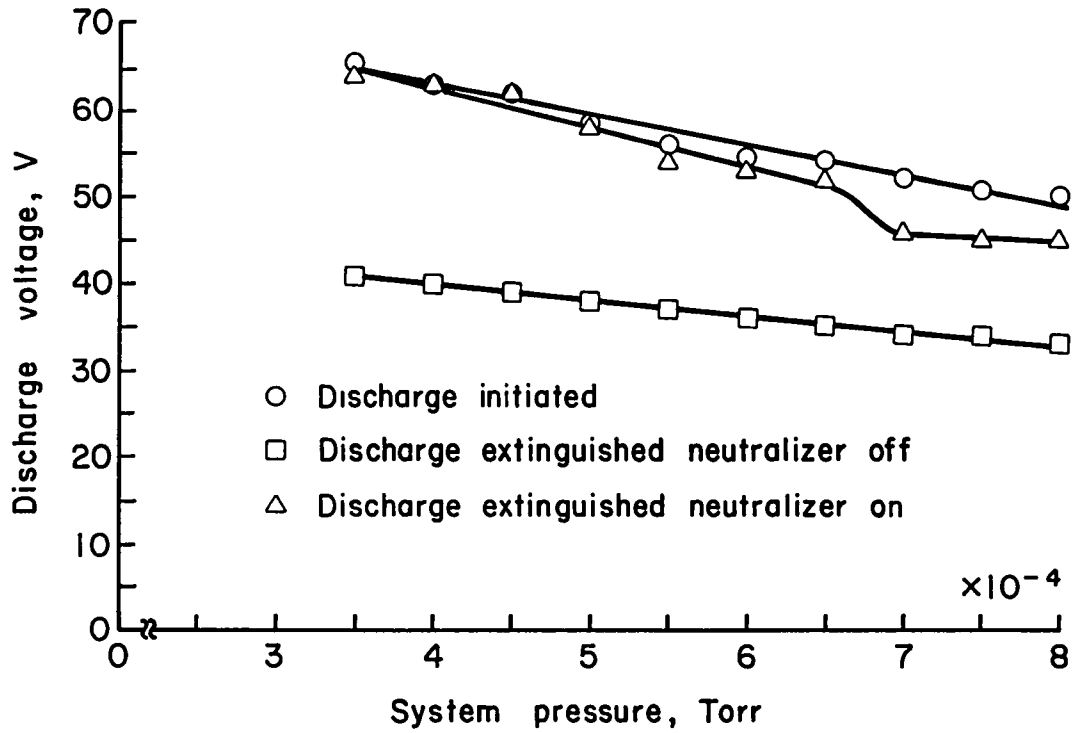

Fig. 13. Anode voltage required to initiate and extinguish the discharge. (When neutralizer on, emission was 1 A. Discharge current 2.5 A.)

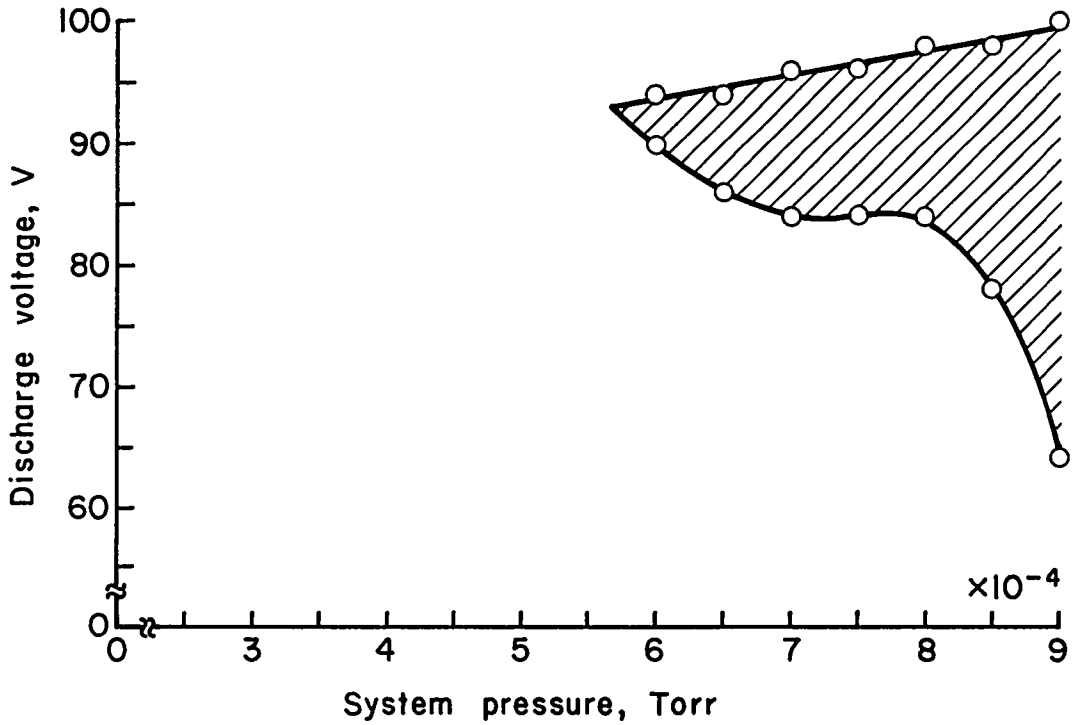

Fig. 14. Range of anode voltages required for operation. (No main cathode, neutralizer cathode emission 1.5 A. Discharge current 2.0 A.)

in Fig. 14. The pressure range of 6-9 × 10^{-4} Torr corresponded to Ar flows of about 600-900 mA-equiv. The minimum pressure of 6.5 × 10^{-4} Torr gave operation at only 94 V, which (in eV) is close to the electron energy for the maximum ionization cross-section of Ar.

The operating ranges for the three-magnet thruster with modified pole pieces, Figs. 15 through 17, indicate at what discharge voltages the discharge initiated and extinguished over a range of system pressures. The main cathode mode was seen to initiate a discharge at a voltage of

$$V = 103 - 6.5 \times 10^4 P \tag{8}$$

and extinguish the discharge at a voltage of

$$V = 44 - 1.6 \times 10^4 P \tag{9}$$

over the range of 3-9 × 10^{-4} Torr. (The data from which Eqs. (8) and (9) were obtained is shown in Fig. 15.) When the neutralizer cathode was also used, at a temperature sufficient to emit 1 A, the discharge initiated at approximately the voltage given in Eq. (8). The voltage at which the discharge was extinguished, however, had two distinctly different slopes at high and low pressures. At low pressures, 3-5 × 10^{-4} Torr, the discharge was extinguished at a voltage of

$$V = 93 - 10.2 \times 10^4 P \tag{10}$$

while at high pressures, 5-9 × 10^{-4} Torr, it extinguished at a voltage approximately the same as in Eq. (9). (The data from which these relationships were obtained are shown in Fig. 16.) While operating in the neutralizer cathode only mode (where the discharge was initiated using the main cathode, which was then turned off) with a neutralizer emission of 2.0 A the discharge extinguished at a voltage of

$$V = 147 - 9.2 \times 10^4 P \quad . \tag{11}$$

(The data from which Eq. (11) was obtained is shown in Fig. 17.)

Comparing the two models it is seen that the neutralizer cathode had a greater adverse effect on the operation in the first model (parallel pole pieces) than it had on the operation of the second model (modified pole pieces) when using both the main cathode and the neutralizer cathode. Also in the neutralizer cathode only mode, the second model did not extinguish at high voltages, as did the first model.

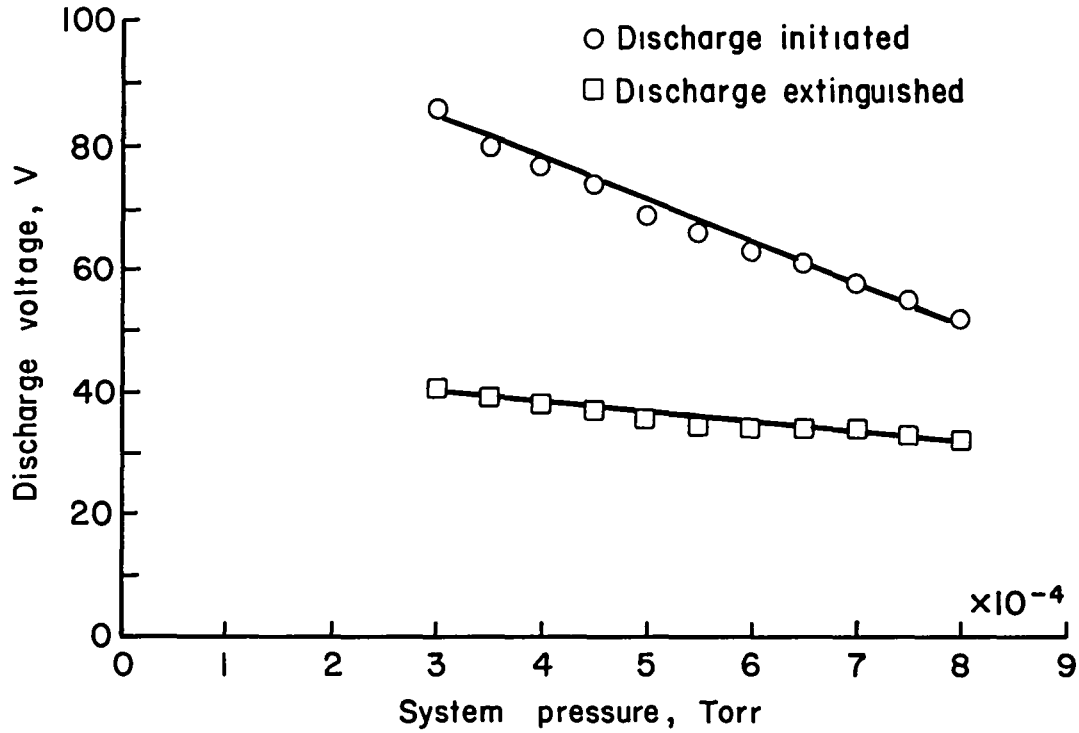

Fig. 15. Anode voltage required to initiate and extinguish the discharge. (No neutralizer cathode emission. Discharge current 2.5 A.)

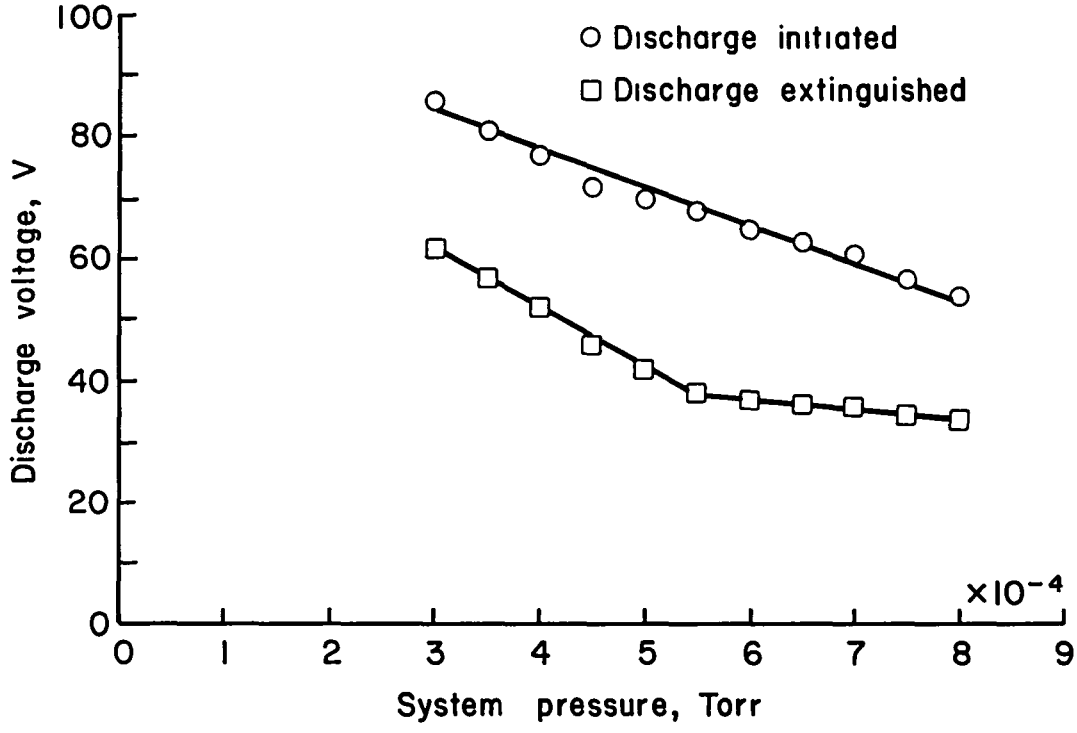

Fig. 16. Anode voltage required to initiate and extinguish the discharge. (Neutralizer emission 1 A. Discharge current 3.5 A.)

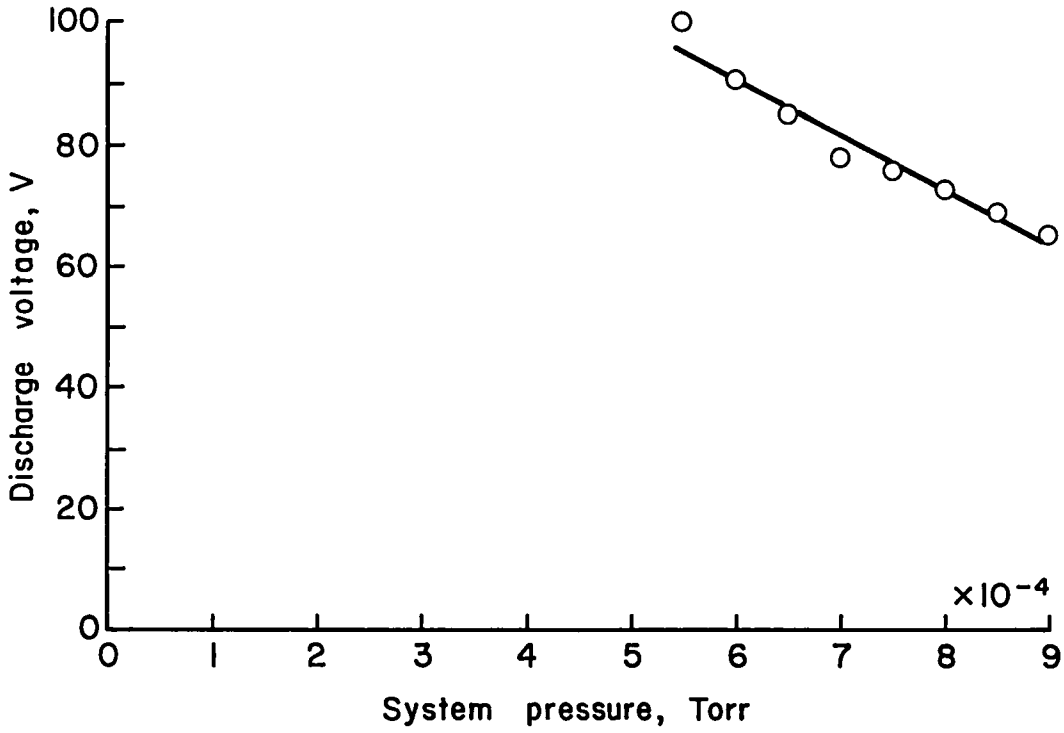

Fig. 17. Anode voltage required to maintain the discharge. No main cathode emission, neutralizer emission 2.0 A. Discharge current 2.5 A.

The interaction between the two cathodes indicated in Figs. 14 and 16 is typical of this investigation. Also simply increasing the neutralizer emission at a fixed main cathode emission and discharge voltage usually resulted in the plasma pulsing or extinguishing, depending on the discharge voltage. On the other hand, if the main cathode emission was reduced as the neutralizer emission was increased, it was occasionally possible to operate at higher neutralizer emissions than otherwise.

Plasma Properties

The plasma properties were profiled using Langmuir probe measurements taken on an axial line at a radius of 1 mm less than that of the main cathode.

Examining the electron distribution by comparing it to the best fit Maxwellian function, Fig. 18 shows that the plasma was not fully thermalized. The "electron temperature" used in this work was the temperature associated with the first peak in the electron distribution.

Note that the absence of a fully thermalized distribution in Fig. 18(b) is consistent with the theoretical approach used for this thruster type.[7] That is, the collisions of the electrons in the enhanced diffusion process were assumed to be primarily with relatively slow-moving ion-plasma waves, moving at ion acoustic velocity. Such collisions would tend to randomize the direction of the electron velocity more rapidly and more fully than the electron energy.

For Fig. 18(a), it is believed that the separate emission from the neutralizer and main cathodes contributed to the multiple peaks. Figure 18(a) data were obtained on the side of the discharge chamber with the 31 G-cm magnetic field integral between the anode and cathode. (Other operating conditions were: pressure, 0.4 mTorr; discharge voltage, 70 V; discharge current, 2.5 A; cathode emission, 1.7 A; and neutralizer emission, 0.6 A.) Thus the primary electrons could not escape easily to the anode. At the same time, the integral from the neutralizer to the probe location was smaller (by the same 11 G-cm). For Fig. 18(b), the reverse was true. One may therefore expect that the neutralizer cathode electrons find it easier to reach the probe through the smaller integral (Fig. 18(a)), and that the emissions from the two sides of the neutralizer corresponded to two of the three distribution peaks.

The plasma properties were profiled for the three-magnet thruster with modified pole pieces (at an operating point of V_d = 70 V, J_d = 2.5 A, J_n = 0.0 A, and P = 0.4 mTorr) to determine the effect of: (1) neutralizer cathode emission, (2) cathode magnetic field, and (3) discharge voltage. The effect of the cathode magnetic field was determined using both the main and neutralizer cathodes, while the effect of the discharge voltage was determined in the neutralizer cathode only mode.

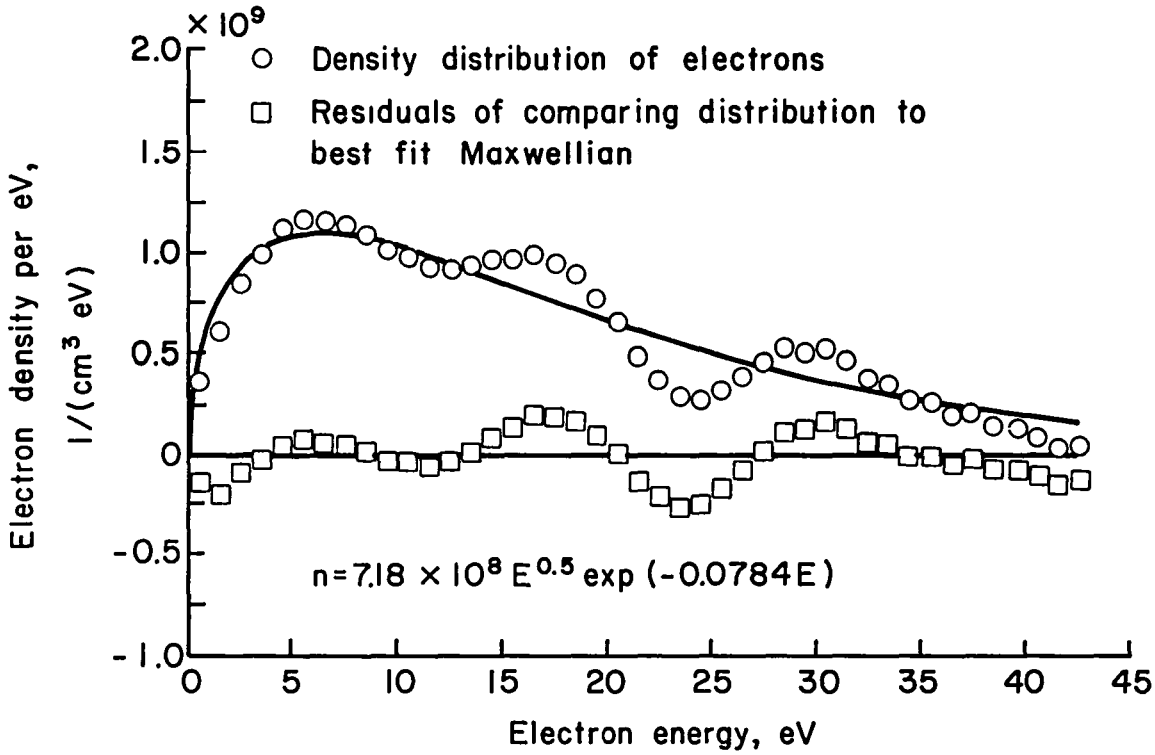

(a) Magnetic integral 3.1×10^{-5} T-m.

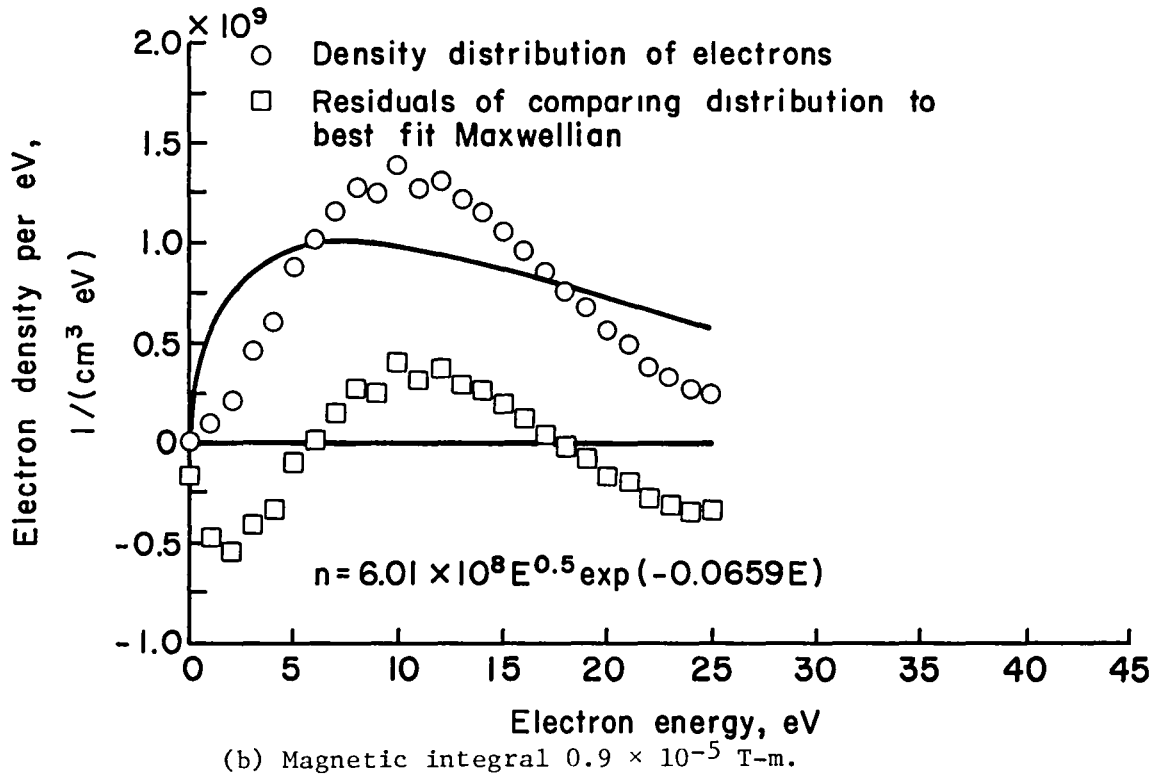

(b) Magnetic integral 0.9×10^{-5} T-m.

Fig. 18. Comparison of the electron distribution with the best fit Maxwellian. (Op. V_d = 70 V, J_d = 2.5 A, J_n = 0.6 A, P = 0.4 mTorr. Probe pos. 2.2 cm from anode, cathode plus 1 mm.)

Operating on main cathode only, Figs. 19 through 21, the plasma potential only dropped by approximately 4 V in leaving the thruster. Also the plasma density peaks within the ionization channel with no secondary peaks, while the electron temperature remained nearly constant.

Operating on both the main and neutralizer cathodes, Figs. 22 through 24, a neutralizer emission of 0.6 A (the operating point remained the same as above except for J_n) decreased the plasma potential downstream of the source by about 25 V. However, it also produced an increase in the plasma density downstream of the exit plane and a decrease of the plasma density inside the ionization channel.

Operating on neutralizer only, Figs. 25 through 27 (operating point was discharge current 2.5 A, neutralizer emission 2.0 A, and pressure 0.4 mTorr) it was seen that the plasma potential difference increased to approximately 35 V. The plasma density downstream of the exit plane, however, was even greater than that inside of the ionization channel.

Using both the main and neutralizer cathodes the effect of the magnetic field, caused by the main cathode heater current, was determined by measuring the plasma properties on both the high and low magnetic integral sides of the ionization channel, Figs. 22 through 24. The combined background and cathode current field for the probe locations are shown in Fig. 10(b). These data show that the cathode magnetic field produces considerable asymmetry in the plasma properties. As mentioned above, these nonuniformities reduce the voltage insulation capabilities of the Hall-current thruster and hence the acceleration efficiency.

The effect of the discharge voltage was examined for neutralizer cathode only operation, Figs. 25 throuth 27. These figures indicate that ion acceleration (difference in plasma potential) was not significantly dependent on the discharge voltage, whereas the electron density increased slightly and the electron temperature decreased with increasing discharge voltage.

The plasma properties were also compared for the three- and six-magnet thrusters with modified pole pieces (on the same axial line as above), Figs. 28 through 30. (The operating conditions were: discharge voltage, 80 V; discharge current, 3.5 A; and pressure, 0.5 mTorr. The neutralizer cathode emission was 0.4 A, Figs. 28(a), 29(a), and 30(a), and 0.8 A, Figs. 28(b), 29(b), and 30(b).)

Results obtained from this profiling indicates that for J_n = 0.4 A, Fig. 28(a), the three-magnet thruster, had a plasma potential difference of approximately 22 V. However, when the neutralizer cathode emission was doubled to J_n = 0.8 A the potential difference increased to approximately 24 V, Fig. 28(b). When the number of magnets was doubled the plasma potential difference for J_n = 0.4 A was approximately 31 V, Fig. 28(a), and when the neutralizer emission was doubled, J_n = 0.8 A, the plasma potential difference increased to approximately 37 V. As shown above, doubling the neutralizer emission from 0.4 A to 0.8 A does not have the same effect on the acceleration potential difference as

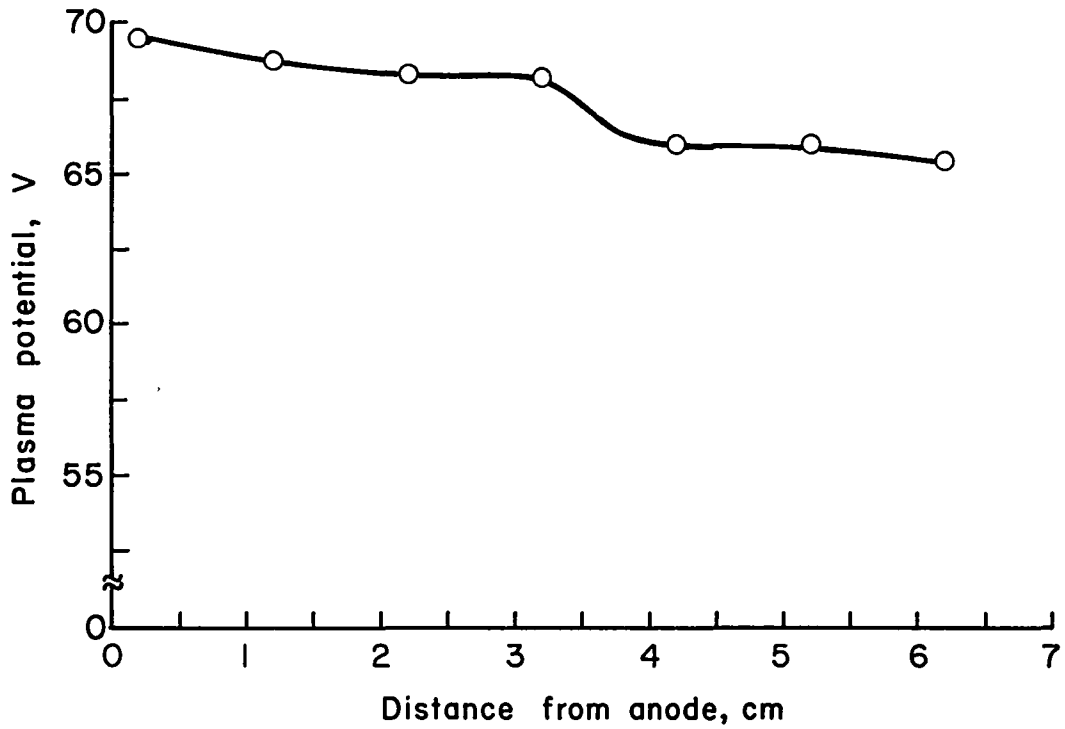

Fig. 19. Plasma potential.

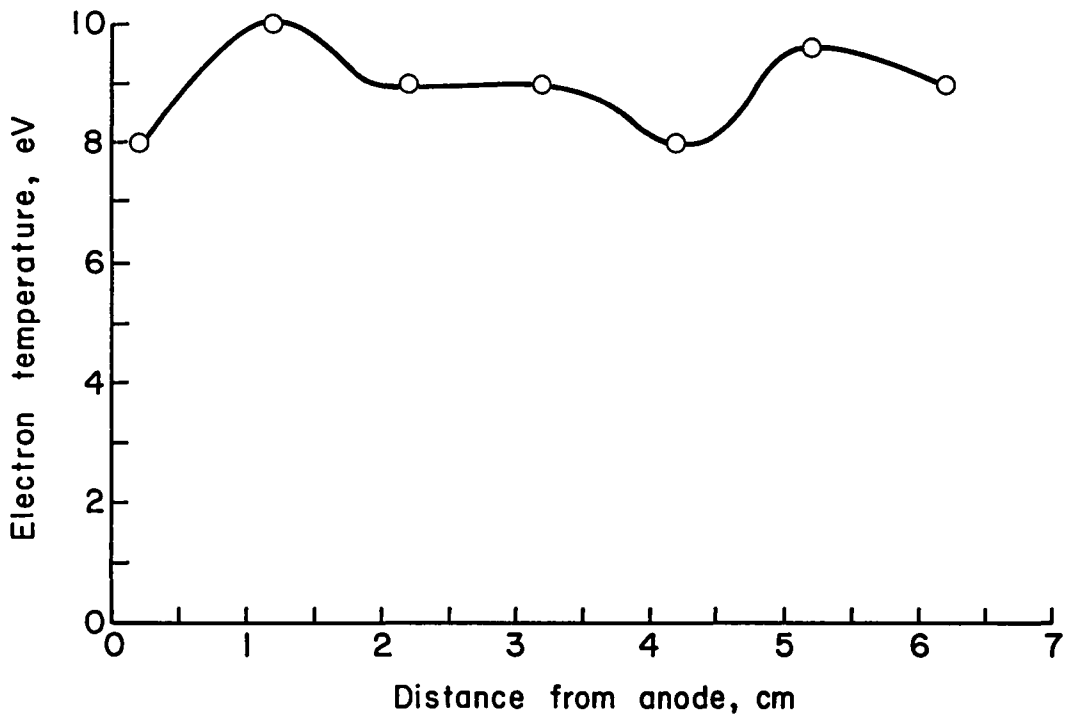

Fig. 20. Electron temperature.

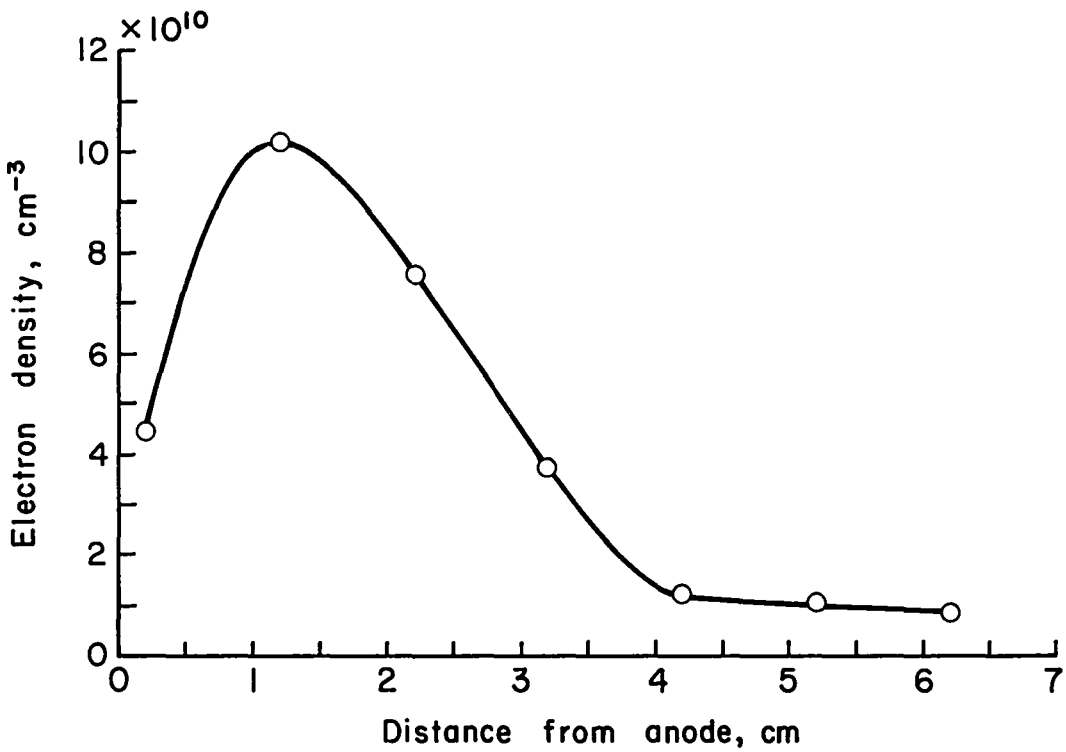

Fig. 21. Electron density.

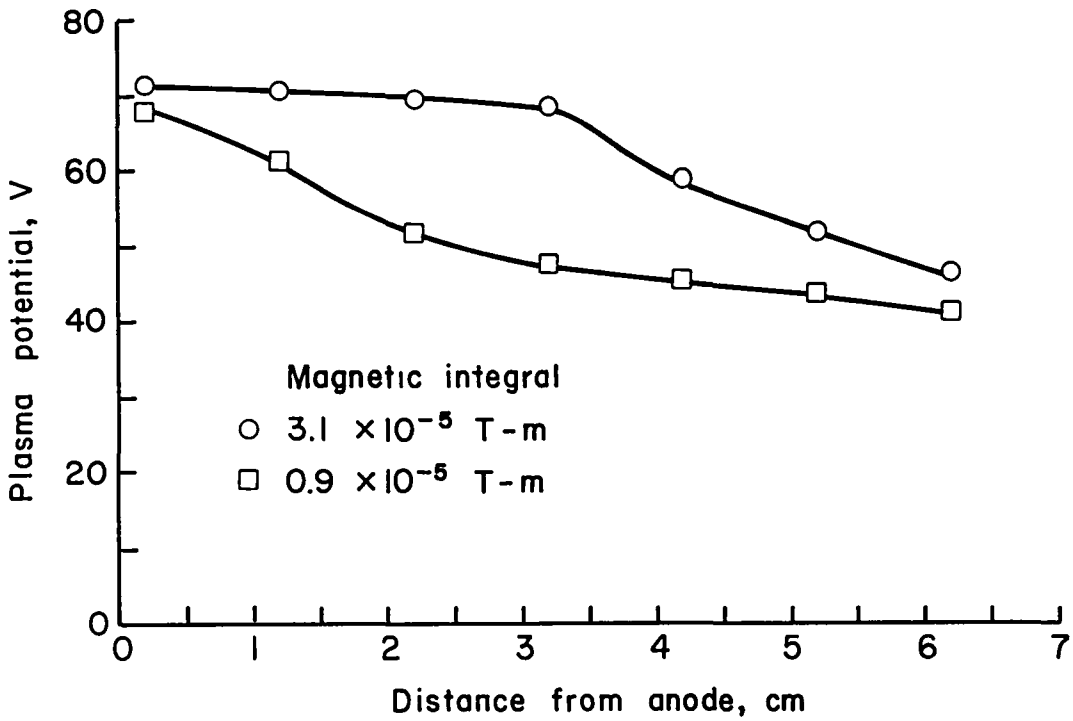

Fig. 22. Plasma potential.

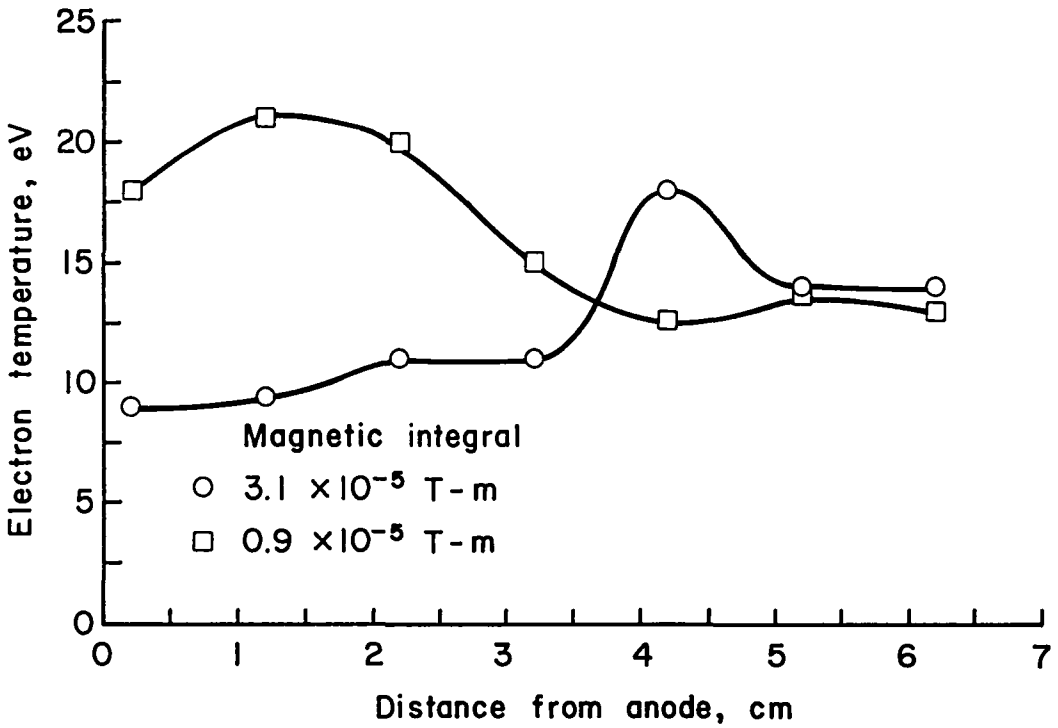

Fig. 23. Electron temperature.

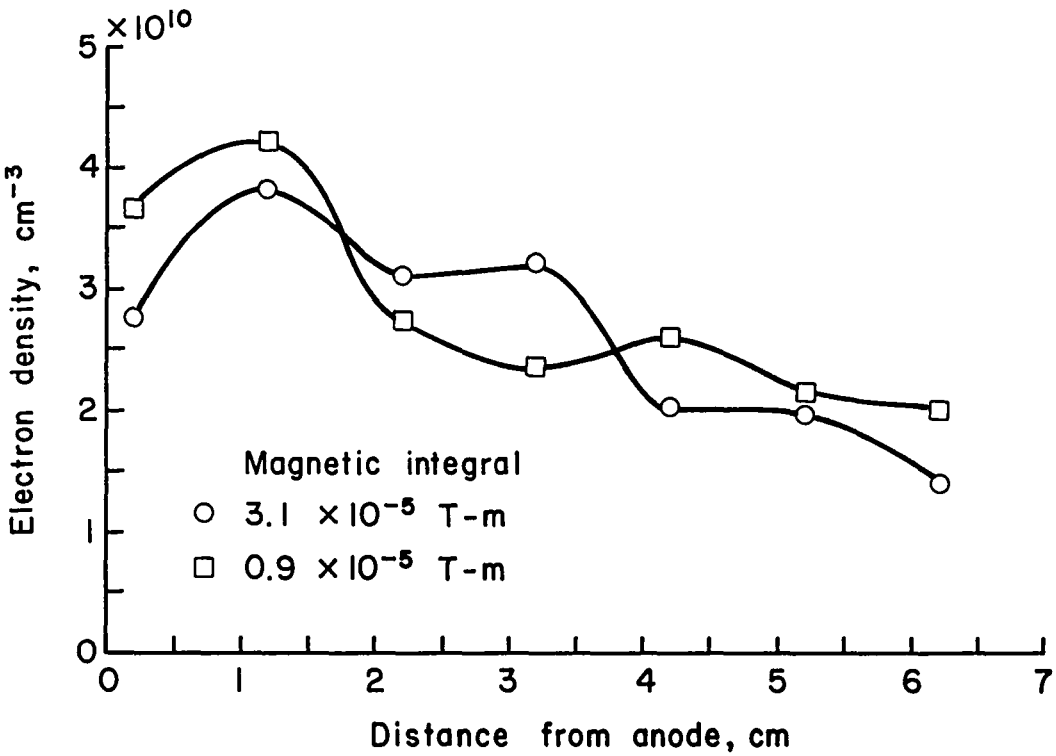

Fig. 24. Electron density.

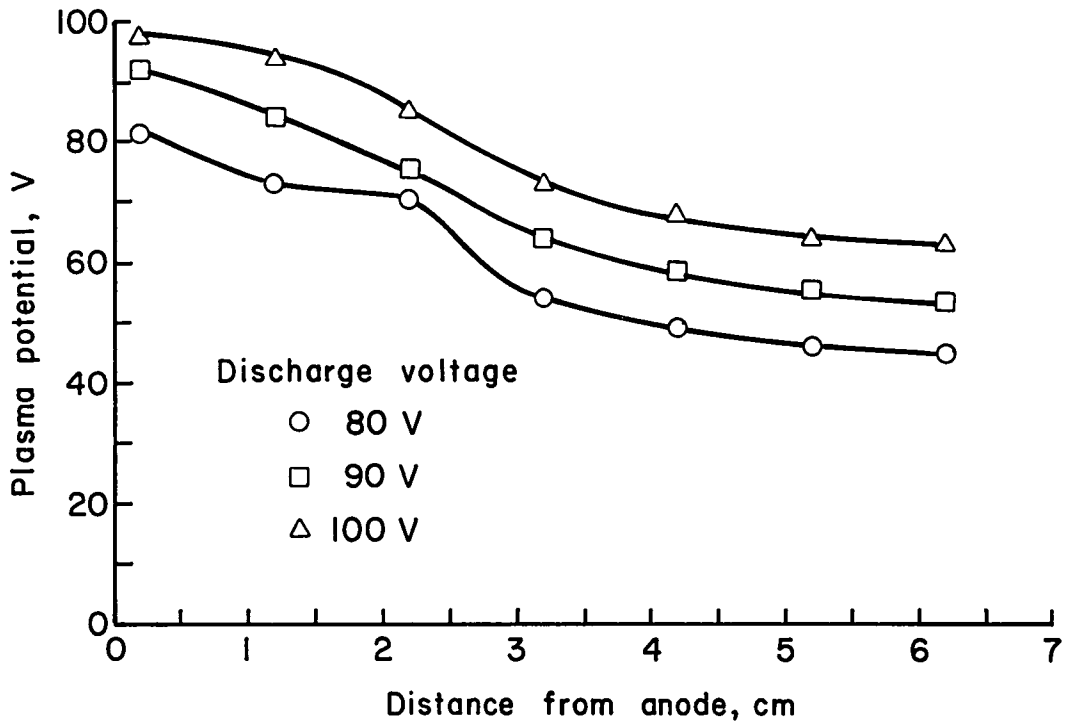

Fig. 25. Plasma potential.

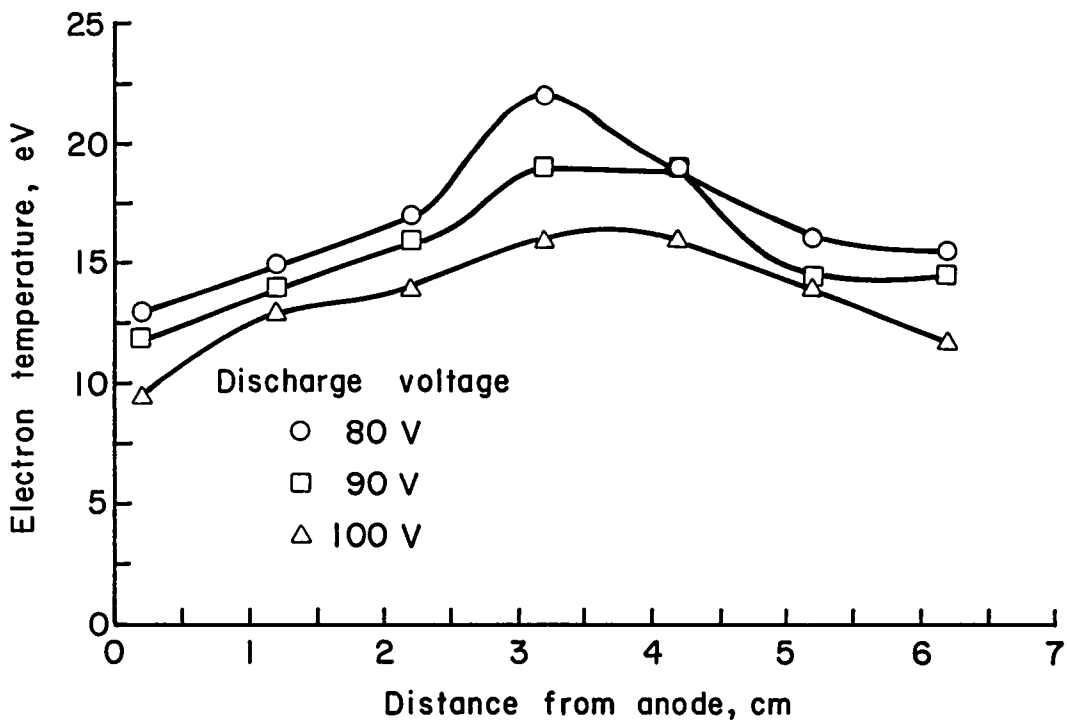

Fig. 26. Electron temperature.

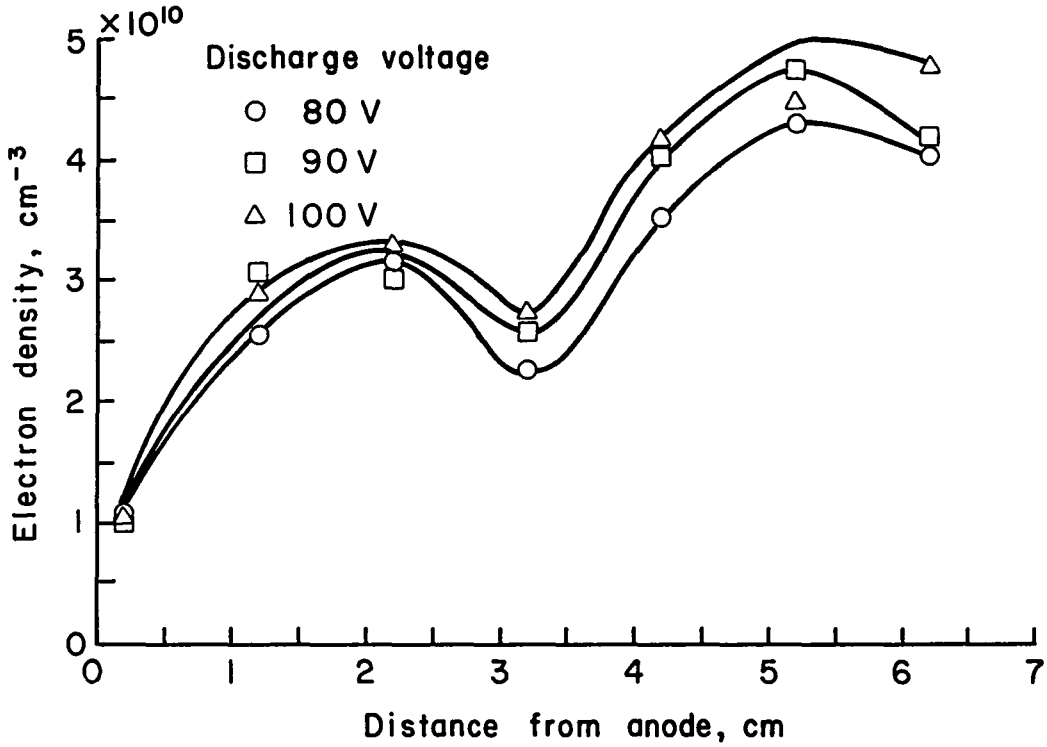

Fig. 27. Electron density.

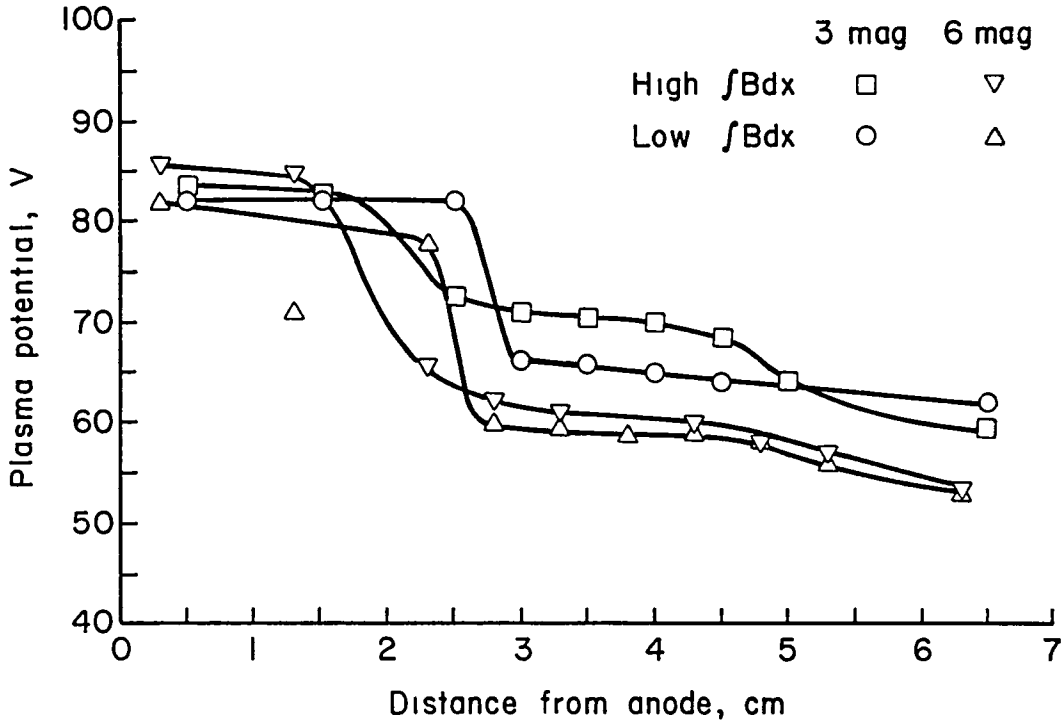

(a) Neutralizer emission = 0.4 A.

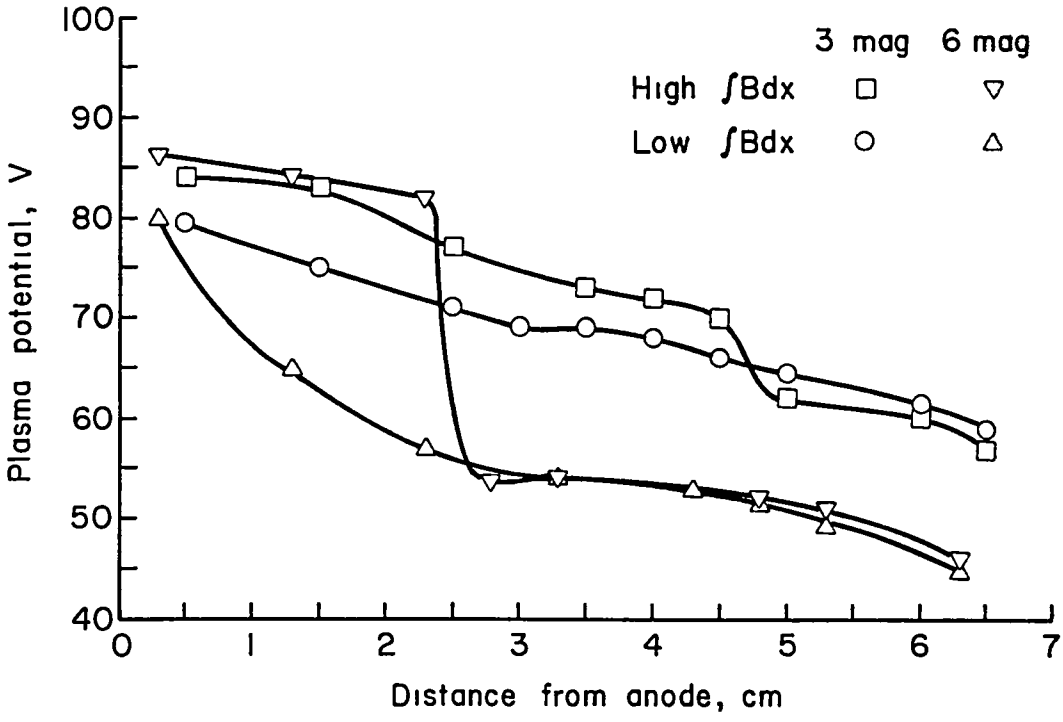

(b) Neutralizer emission = 0.8 A.

Fig. 28. Plasma potential, three and six magnet thrusters with modified poles. (Op. V_d = 80 V, J_d = 3.5 A, P = 0.5 mTorr.)

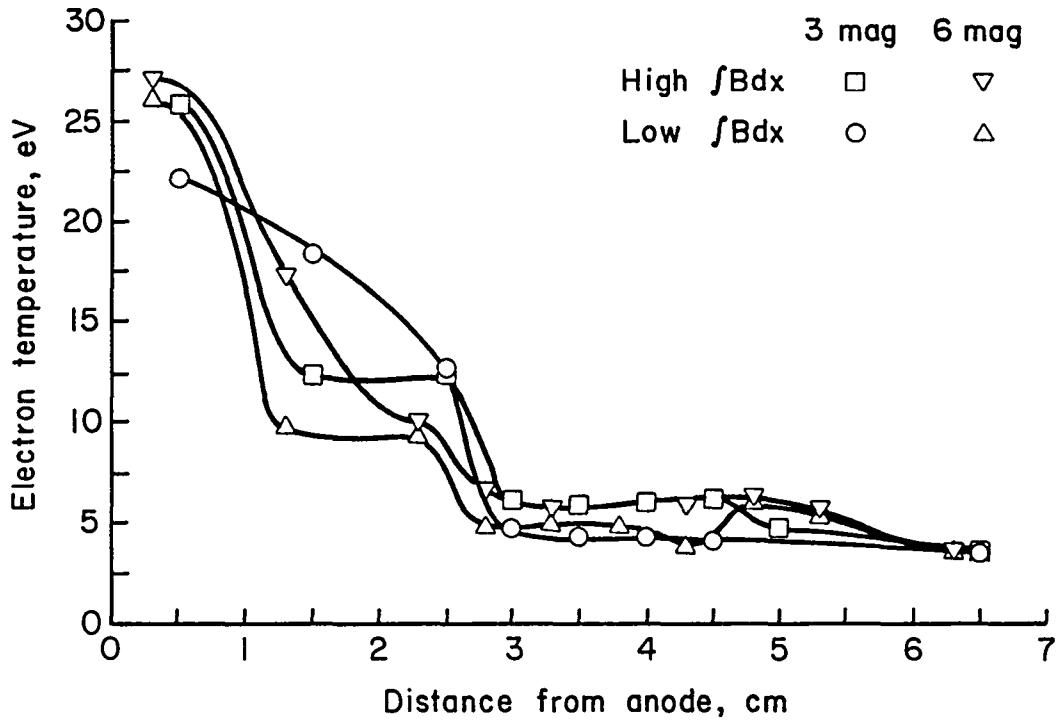

(a) Neutralizer emission = 0.4 A.

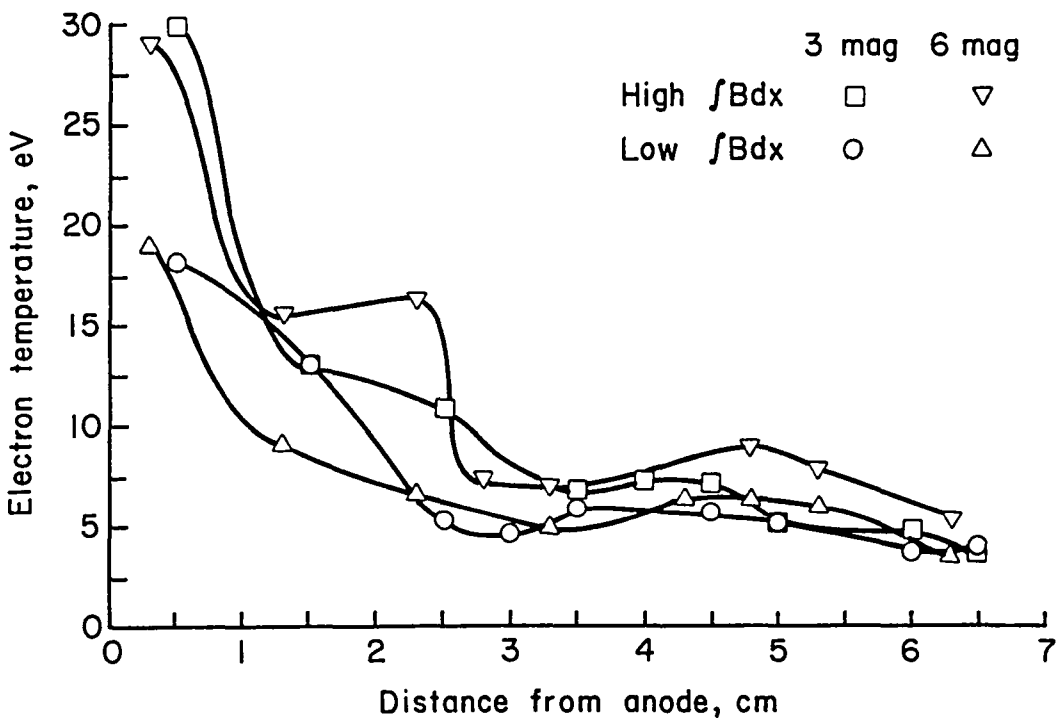

(b) Neutralizer emission = 0.8 A.

Fig. 29. Electron temperature, three and six magnet thrusters with modified poles. (Op. V_d = 80 V, J_d = 3.5 A, P = 0.5 mTorr.)

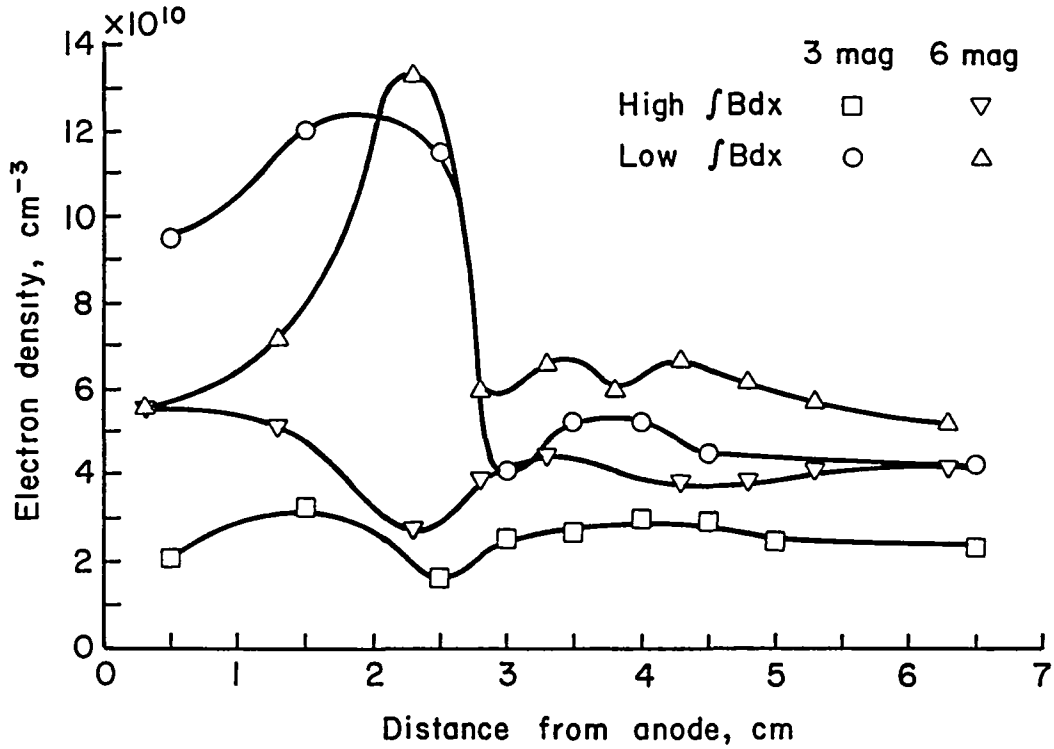

(a) Neutralizer emission = 0.4 A.

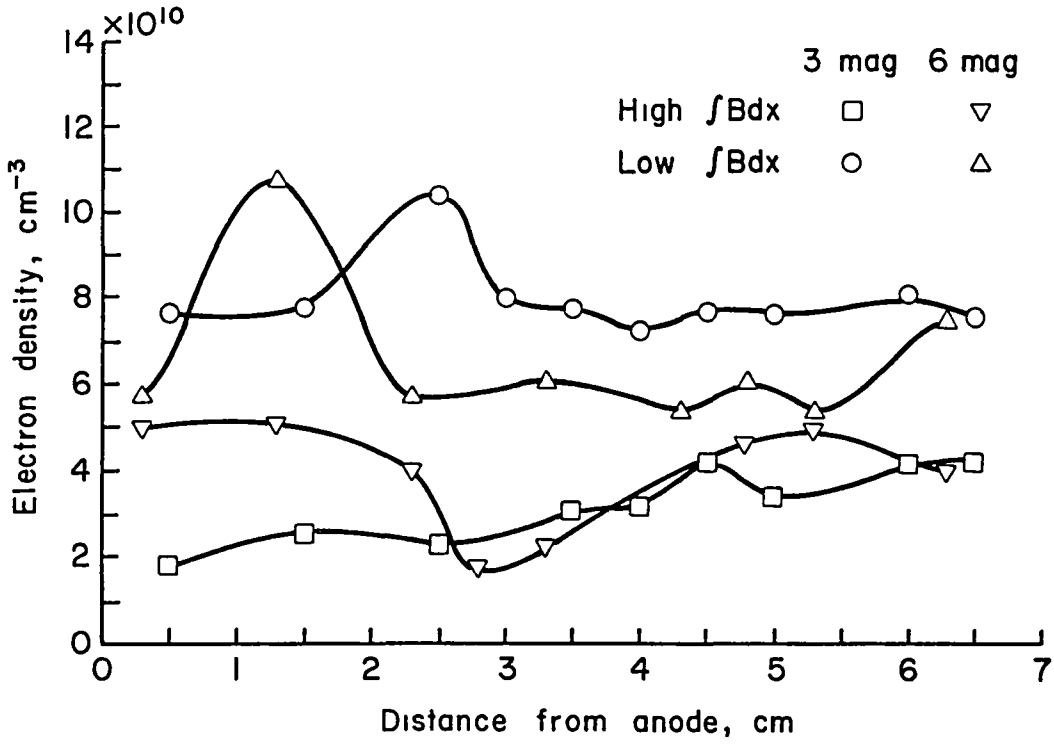

(b) Neutralizer emission = 0.8 A.

Fig. 30. Electron density, three and six magnet thrusters with modified poles. (Op. V_d = 80 V, J_d = 3.5 A, P = 0.5 mTorr.)

does doubling the number of magnets from three to six. In Fig. 29(b) it is shown that the high magnetic field integral side (high integral between anode and cathode, low integral between main cathode and exit plane) had a higher electron temperature than the low integral side for J_n = 0.8 A. This effect was much less for the lower neutralizer emission of 0.4 A shown in Fig. 29(a). All curves, however, converged to approximately 3.7 eV at 6.5 cm from the anode. It is also shown in Figs. 30(a) and 30(b) that the electron density was greater on the low magnetic field integral side than on the high integral side. This effect was also more pronounced at the higher neutralizer emission. However, the electron-plasma density showed little tendency to converge over the surveyed region.

Beam Characteristics

The beam can be characterized by three parameters, the beam current, Fig. 31, the average beam energy, Fig. 32, along with the beam divergence angle. The beam divergence angle is that half angle which subtends 95% of the beam. These beam parameters were found by using a Faraday cup to obtain an energy and density profile of the beam. The beam divergence for the three- and six-magnet thruster with modified pole pieces was measured at approximately 14°. As shown in Fig. 31, the three-magnet thruster provided approximately three times the beam current as the six-magnet thruster. The beam current peaked for the three-magnet thruster at about 1000 mA giving a beam current density of approximately 18 mA/cm^2. The average beam energy was lower for the six-magnet thruster than for the three-magnet thruster, giving the three-magnet thruster not only a greater beam but also a higher energy beam than the six-magnet thruster. The beam current density was also found to fall off with distance at approximately the rate predicted by charge exchange taking place with the background gas.[10]

The possibility of double ions in the beam giving a higher beam current measurement than could be accounted for by assuming singly ionized Ar was also considered. This was estimated by using the method developed to calculate double ion production in electrostatic thrusters.[11] It was found that for a discharge voltage of 80 V, approximately 6.5% of the beam current could be due to double ions.

Thruster Characteristics

The thruster performance can be characterized by the energy cost per ion, Fig. 33, and the thrust provided, Fig. 34. As shown in Fig. 33 the energy cost per ion for the six-magnet thruster was much greater than that of the three-magnet thruster. Also from Fig. 34 it can be seen that the three-magnet thruster provided much more thrust than the six-magnet thruster.

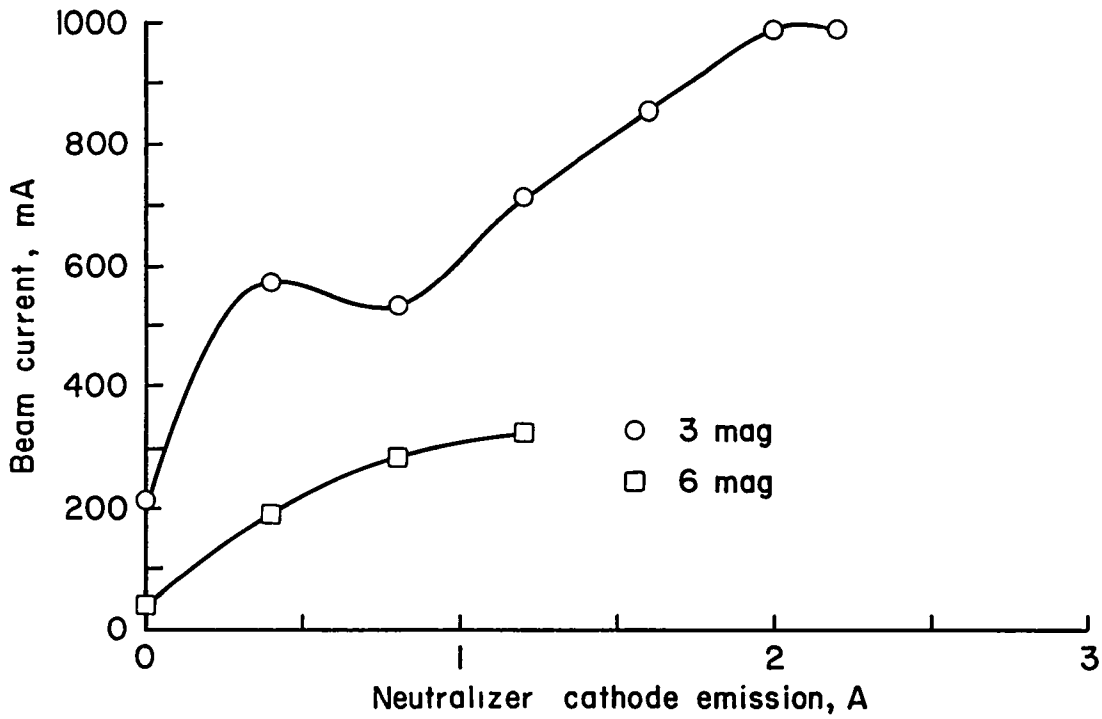

Fig. 31. Total beam current at exit plane of thrusters. (Op. V_d = 80 V, J_d = 3.5 A, P = 0.5 mTorr.)

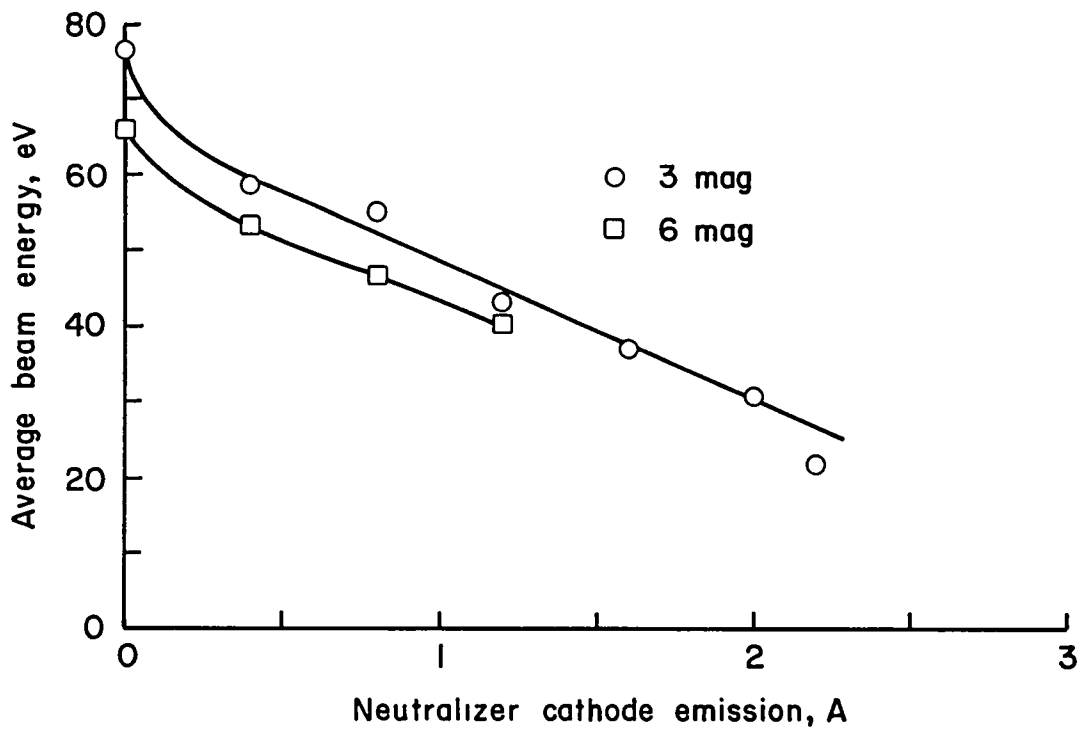

Fig. 32. Average discharge energy of the beam ions. (Op. V_d = 80 V, J_d = 3.5 A, P = 0.5 mTorr.)

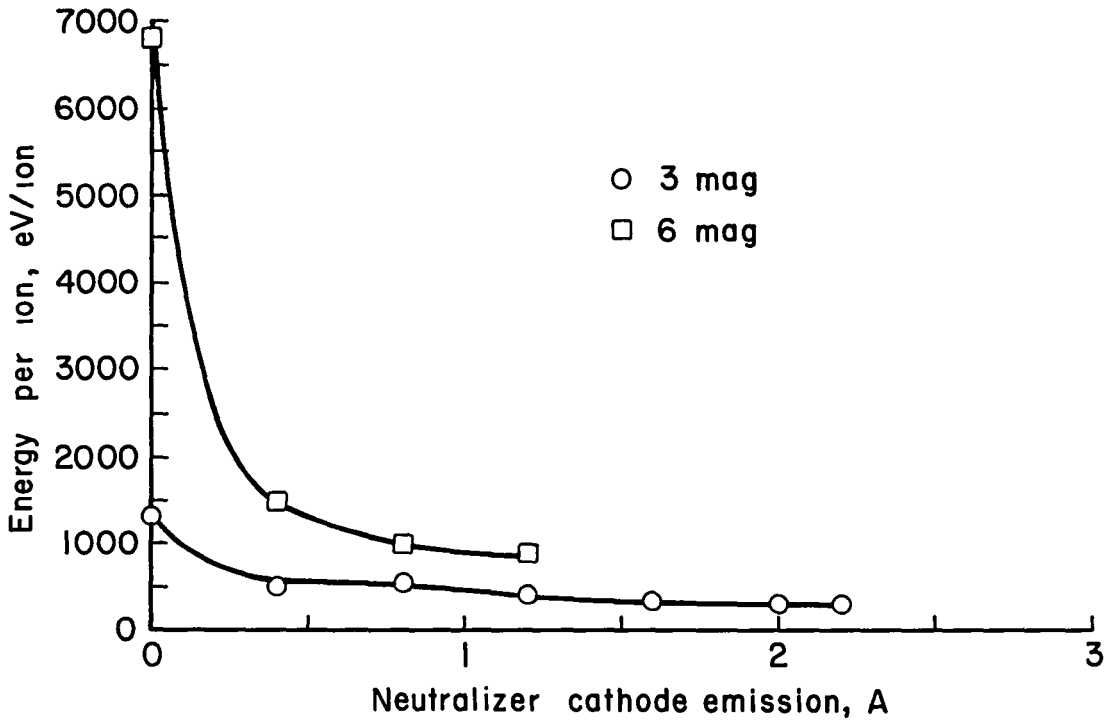

Fig. 33. Average energy cost per beam ion. (Op. V_d = 80 V, J_d = 3.5 A, P = 0.5 mTorr.)

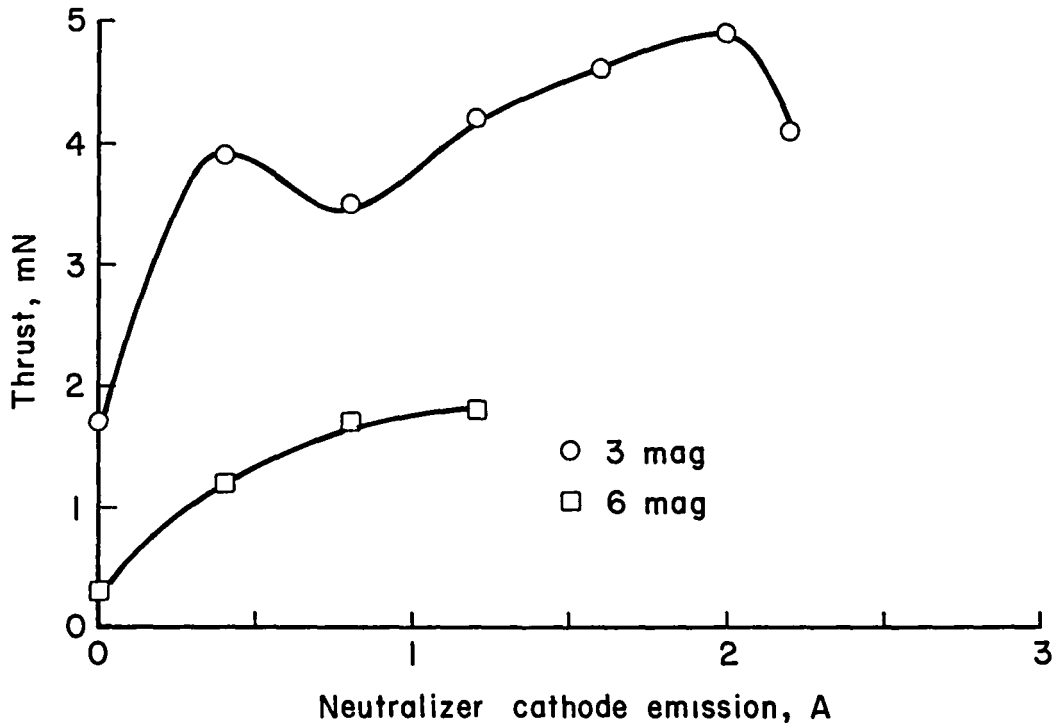

Fig. 34. Total thrust of the Hall-current accelerators. (Op. V_d = 80 V, J_d = 3.5 A, P = 0.5 mTorr.)

CONCLUSIONS

Three experimental Hall-current thrusters were tested with refractory metal cathodes, where the major differences in the thrusters were in the magnetic field, both the strength and/or the axial uniformity of the magnetic field. The magnetic field integral between the anode and cathode was reduced from an initial value of 50-60 $\times 10^{-6}$ T-m to 20 $\times 10^{-6}$ T-m to facilitate starting and operation at low voltages (<100 V).

The use of refractory metal cathodes resulted in serious circumferential variations in the magnetic field, which resulted in corresponding variations in plasma properties. Some of the limited voltage isolation capability observed was probably due to the adverse affects of the refractory cathode on circumferential uniformity.

The higher magnetic field offered by the six-magnet thruster, while increasing the voltage isolation capabilities beyond that of the three-magnet thruster, also severely reduced the total beam current that the thruster would deliver. The higher magnetic field also reduced the average energy of the beam. Both reduced beam current and the lower average energy contribute to the six-magnet thruster having less thrust and a higher energy cost per ion than the three-magnet thruster.

Various operating modes were possible with the main and neutralizer cathodes. Operation with the neutralizer cathode only, however, was severely hampered by the high system pressures necessary to maintain a discharge. Operating at these high pressures, there was a tendency for a plasma arc to become established with surrounding hardware, preventing normal thruster operation. It was found that the thruster generally produced a higher beam current at higher neutralizer emissions. But as the neutralizer emission increased, the average energy in the beam also decreased. Since the increase in beam current with neutralizer cathode emission was greater than the decrease of average energy, the thruster produced the maximum thrust when the neutralizer cathode supplied most but not all of the discharge current.

As major conclusions, then, the heating current for a refractory metal cathode adversely affect the circumferential uniformity in a Hall-current thruster. The optimum magnetic field was within the range of our experiments and thus easily achievable. The optimum operating condition with both cathodes would be achieved when the neutralizer cathode supplies approximately 70% of the discharge current with the main cathode supplying the remainder. It was also found that a low magnetic field strength results in inadequate voltage isolation for ion acceleration. Thus having made no attempt to optimize the performance, and working at a discharge of 80 V and 3.5 A the three-magnet

thruster with modified poles produced a beam with an ion current density of approximately 18 mA/cm^2 with an average beam energy of 31 eV which gave a thrust of about 5 mN with a specific impulse of approximately 1300 sec. using a discharge energy of about 280 eV/ion.

One approach for avoiding the field-strength problem in which the field strength must be reduced for starting is to have a "discharge chamber" upstream of the acceleration region, so that the ion generation can take place with only moderate field strengths in this region, while high field strengths are still maintained in the acceleration region. This is the general approach used in Hall-current accelerators in the U.S.S.R.[4]

Another approach might be to use more sophisticated approaches to electron diffusion in the "discharge chamber" region. Electron-bombardment thrusters have discharge problems when the magnetic integral between the anode and main cathode become too large. This problem is aggravated when the anode area is only a small fraction of the total wall area of the discharge chamber.[12] It is suspected both of these factors are involved in field-strength problems encountered in this investigation. Inasmuch as the diffusion of electrons to the anode is the common limit when too high an integral or too small an anode area is used, alternate mechanisms for electrons may effectively solve these problems.

REFERENCES

1. Staff of NASA Lewis Research Center, "30-cm Ion Thruster Subsystem Design Manual," NASA Tech. Mem. TM-79191, June 1979.

2. H. R. Kaufman, "Performance of Large Inert-Gas Thrusters," AIAA Paper No. 81-0720, April 1981. (A closely related paper is H. R. Kaufman and R. S. Robinson, "Large Inert-Gas Thrusters," AIAA Paper No. 81-1540, July 1981.)

3. H. R. Kaufman and R. S. Robinson, "Electric Thruster Performance for Orbit Raising and Maneuvering," AIAA Paper No. 82-1247, June 1982.

4. Papers of IV All-Union Conf. on Plasma Accelerators and Ion Injectors, Moscow, 1979 (in Russian).

5. M. C. Ellis, Jr., "Survey of Plasma Accelerator Research," in Proc. NASA - University Conference on the Science and Technology of Space Exploration - Vol. 2, NASA, Washington, D.C., pp. 361-381, November 1962.

6. G. S. Janes and R. S. Lowder, "Anomalous Electron Diffusion and Ion Acceleration in a Low-Density Plasma," Phys. Fluids, Vol. 9, pp. 1115-1123, June 1966.

7. H. R. Kaufman, "Theory of Ion Acceleration with Closed Electron Drift," AIAA Paper No. 82-1919, November 1982.

8. R. H. Huddlestone and S. L. Leonard, Plasma Diagnostic Techniques, Academic Press, Inc., New York, 1965, Ch. 4.

9. Y. Takeishi and H. D. Hagstram, Phys. Rev. 137A, 641 (1965).

10. R. S. Robinson, "Physical Processes in Directed Ion Beam Sputtering," NASA Contr. Rep. CR-159567, March 1979.

11. R. R. Peters, "Double Ion Production in Mercury Thrusters," NASA Contr. Rep. CR-135019, April 1976.

12. H. R. Kaufman and R. S. Robinson, "Ion Source Design for Industrial Application," AIAA Paper No. 81-0668, April 1981. (Also NASA Contr. Rep. CR-165334, January 1981.)

End of Document